Cell Reports

Article

Post-transcriptional Gene Regulation by MicroRNA-194 Promotes Neuroendocrine Transdifferentiation in Prostate Cancer

Graphical Abstract

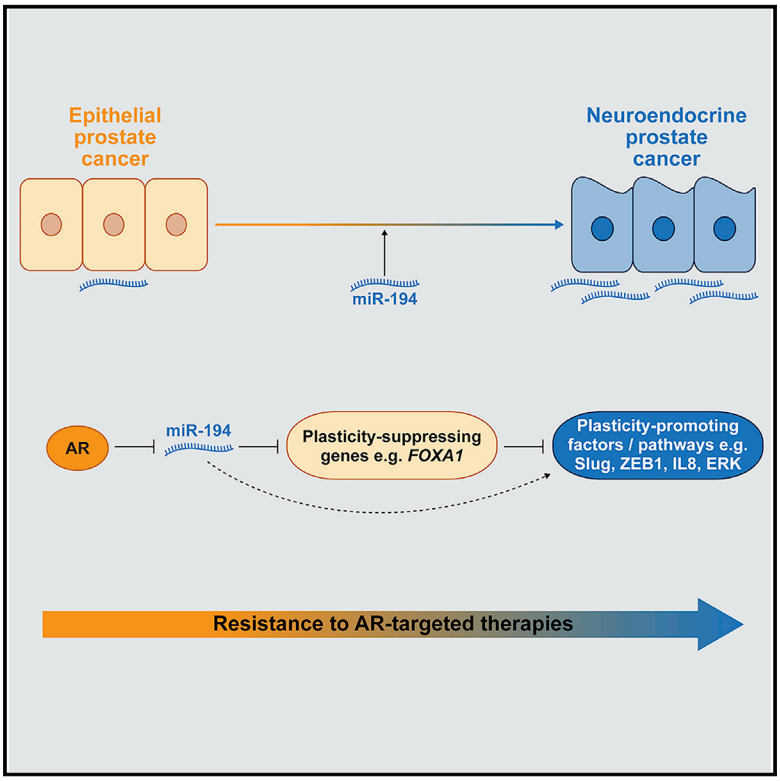

Authors

Rayzel C. Fernandes, John Toubia, Scott Townley, ..., Theresa E. Hickey, Gregory J. Goodall, Luke A. Selth

Correspondence

luke.selth@flinders.edu.au

In Brief

Neuroendocrine prostate cancer is an aggressive disease subtype associated with poor patient outcome. Fernandes et al. demonstrate that a microRNA, miR-194, promotes the emergence of neuroendocrine features in prostate cancer cells by targeting genes that regulate epithelial-neuroendocrine plasticity. Inhibiting miR-194 suppresses the growth of neuroendocrine prostate cancer models.

Highlights

- miR-194 promotes the emergence of neuroendocrine features in prostate cancer
- miR-194 is negatively associated with androgen receptor signaling
- miR-194 targets a network of genes to enhance epithelial-neuroendocrine plasticity
- Targeting miR-194 inhibits the growth of prostate cancer with neuroendocrine features

Fernandes et al., 2021, Cell Reports *34*, 108585
January 5, 2021
https://doi.org/10.1016/j.celrep.2020.108585

CellPress

Cell Reports

CellPress
OPEN ACCESS

Article

Post-transcriptional Gene Regulation by MicroRNA-194 Promotes Neuroendocrine Transdifferentiation in Prostate Cancer

Rayzel C. Fernandes,[1] John Toubia,[2] Scott Townley,[1] Adrienne R. Hanson,[1] B. Kate Dredge,[3] Katherine A. Pillman,[3] Andrew G. Bert,[3] Jean M. Winter,[1] Richard Iggo,[1,4] Rajdeep Das,[1,5] Daisuke Obinata,[6,7] MURAL investigators,[7,8] Shahneen Sandhu,[8,9] Gail P. Risbridger,[7,8,9] Renea A. Taylor,[8,10] Mitchell G. Lawrence,[7,8] Lisa M. Butler,[11,12] Amina Zoubeidi,[13] Philip A. Gregory,[3,12] Wayne D. Tilley,[1] Theresa E. Hickey,[1] Gregory J. Goodall,[3,14] and Luke A. Selth[1,15,16,*]

[1]Dame Roma Mitchell Cancer Research Laboratories and Freemasons Foundation Centre for Men's Health, Adelaide Medical School, The University of Adelaide, Adelaide, SA 5005, Australia
[2]ACRF Cancer Genomics Facility, Centre for Cancer Biology, An alliance of SA Pathology and University of South Australia, Frome Road, Adelaide, SA 5005, Australia
[3]Centre for Cancer Biology, An alliance of SA Pathology and University of South Australia, Adelaide, SA 5005, Australia
[4]Institut Bergonié Unicancer, INSERM U1218, Bordeaux, France
[5]Transplant Immunology Laboratory, Comprehensive Transplant Center, Northwestern University Feinberg School of Medicine, Chicago, IL 60611, USA
[6]Department of Urology, Nihon University School of Medicine, Tokyo 173-8610, Japan
[7]Department of Anatomy and Developmental Biology, Monash Partners Comprehensive Cancer Consortium, Monash Biomedicine Discovery Institute, Prostate Cancer Research Group, Monash University, Clayton, VIC 3168, Australia
[8]Cancer Research Program, Cancer Research Division, Peter MacCallum Cancer Centre, University of Melbourne, Melbourne, VIC 3000, Australia
[9]Sir Peter MacCallum Department of Oncology, The University of Melbourne, Parkville, VIC 3000, Australia
[10]Department of Physiology, Monash Partners Comprehensive Cancer Consortium, Monash Biomedicine Discovery Institute, Prostate Cancer Research Group, Monash University, Clayton, VIC 3168, Australia
[11]South Australian Health and Medical Research Institute, Adelaide, SA 5000, Australia
[12]Faculty of Health and Medical Sciences, The University of Adelaide, Adelaide, SA 5005, Australia
[13]The Vancouver Prostate Centre, University of British Columbia, Vancouver, BC V6H 3Z6, Canada
[14]School of Biological Sciences, The University of Adelaide, Adelaide, SA 5005, Australia
[15]Flinders Health and Medical Research Institute, Flinders University, Bedford Park, SA 5042, Australia
[16]Lead Contact
*Correspondence: luke.selth@flinders.edu.au
https://doi.org/10.1016/j.celrep.2020.108585

SUMMARY

Potent therapeutic inhibition of the androgen receptor (AR) in prostate adenocarcinoma can lead to the emergence of neuroendocrine prostate cancer (NEPC), a phenomenon associated with enhanced cell plasticity. Here, we show that microRNA-194 (miR-194) is a regulator of epithelial-neuroendocrine transdifferentiation. In clinical prostate cancer samples, miR-194 expression and activity were elevated in NEPC and inversely correlated with AR signaling. miR-194 facilitated the emergence of neuroendocrine features in prostate cancer cells, a process mediated by its ability to directly target a suite of genes involved in cell plasticity. One such target was *FOXA1*, which encodes a transcription factor with a vital role in maintaining the prostate epithelial lineage. Importantly, a miR-194 inhibitor blocked epithelial-neuroendocrine transdifferentiation and inhibited the growth of cell lines and patient-derived organoids possessing neuroendocrine features. Overall, our study reveals a post-transcriptional mechanism regulating the plasticity of prostate cancer cells and provides a rationale for targeting miR-194 in NEPC.

INTRODUCTION

Cellular plasticity, also referred to as lineage plasticity or lineage switching, is a process whereby cells exhibit reversible changes in properties and phenotypes. Cancer cells exploit this phenomenon in response to a targeted therapy, acquiring the phenotypic characteristics of another lineage that does not depend on the drug target for survival (Davies et al., 2018). This phenomenon allows cancer cells to adapt to new or stressful conditions and is increasingly recognized as a key feature of cancer progression (Yuan et al., 2019).

As first-line treatment for metastatic prostate cancer (PCa), androgen deprivation therapy targets the exquisite dependence of tumors on the androgen receptor (AR) for their growth. Although the therapy is initially effective, patients inevitably develop resistance and progress to castration-resistant prostate cancer (CRPC). Most CRPC tumors exhibit adaptive changes that maintain AR activity despite the low androgen environment, an understanding that led to the development of highly potent second-generation AR-targeted therapies (e.g., enzalutamide and abiraterone). However, response to these newer agents is also limited in most cases (Recine and Sternberg, 2015). It has become increasingly clear that prolonged targeting of the AR, particularly with the more potent second-generation therapies, can drive cellular plasticity in CRPC. This plasticity is characterized by cells losing dependence on AR and gaining new phenotypes (i.e., aggressive variant PCa), with the most well recognized of these being a neuroendocrine (NE)-like state that is characterized by the expression of NE, neuronal, developmental, and stem cell markers (Davies et al., 2018). NE prostate cancer (NEPC) is evident in ~15%–25% of CRPC tumors (Aggarwal et al., 2018; Aparicio et al., 2011) and exhibits aggressive clinical features; indeed, patients with NEPC have a median overall survival time of <1 year (Aggarwal et al., 2018). A deeper understanding of how AR-targeted therapies promote lineage plasticity and the emergence of aggressive disease phenotypes such as NEPC is essential to improve patient outcomes.

Genomic comparisons of NEPC and CRPC adenocarcinoma (CRPC-Adeno) have revealed surprisingly few genetic differences between these disease subtypes; reproducible alterations in NEPC include higher incidences of *RB1* and *TP53* loss and more frequent amplification of *MYCN* and *AURKA* (Beltran et al., 2011, 2016). The similarities in mutational landscapes between NEPC and CRPC-Adeno suggest that the plasticity underlying transdifferentiation from adenocarcinoma to an NE-like state is predominantly mediated by changes in epigenetics, transcriptional programs, and protein function in the tumor cells, as opposed to selection and outgrowth of rare genetic variants (Davies et al., 2018).

Alterations to the expression and activity of lineage-defining transcription factors is an important regulator of epithelial-NE transdifferentiation (Davies et al., 2020). For example, loss of FOXA1, which plays a key role in maintaining the epithelial cell state, has been reported to occur during the development of NEPC (Kim et al., 2017). FOXA1 is a critical regulator of AR signaling in normal prostate development and during carcinogenesis; in the latter context, it reprograms AR binding to promote oncogenic transcriptional programs (Robinson et al., 2014; Pomerantz et al., 2015). FOXA1 also acts independently of AR to repress pro-plasticity factors including interleukin-8 (IL-8), SLUG, and TGFB3 (Kim et al., 2017; Song et al., 2019; Jin et al., 2013), which may at least partly explain its negative association with NEPC.

Like transcription factors, microRNAs (miRNAs) also play a key role in fine-tuning transcriptional networks. miRNA-194 (miR-194) was initially identified as a circulating marker of PCa that was predictive of disease recurrence following surgery (Selth et al., 2013) and subsequently shown to promote metastasis of prostate cancer cells (Das et al., 2017). However, the genes and networks miR-194 regulates remain largely unknown. In this study, we demonstrated that miR-194 acts as a post-transcriptional regulator of transdifferentiation in PCa. By targeting genes that suppress plasticity, such as *FOXA1*, miR-194 drives the emergence and growth of NEPC, a finding that justifies further investigation of miRNA-based therapies for this aggressive CRPC subtype.

RESULTS

Global Identification of Transcripts Targeted by miR-194 in Prostate Cancer

Our earlier work demonstrated that miR-194 can promote epithelial-mesenchymal transition (EMT) and metastasis, at least in part by targeting the tumor suppressor SOCS2 (Das et al., 2017). However, miRNAs target tens to hundreds of genes, so we hypothesized that elucidating additional miR-194 targets would shed further light on its oncogenic functions in PCa. Thus, we performed Ago-HITS-CLIP on control- and miR-194-transfected 22Rv1 PCa cells to decode miRNA-mRNA interactions. The 22Rv1 model was chosen for this discovery experiment because it exhibited increased metastatic capacity upon transient delivery of miR-194 (Das et al., 2017). After immunoprecipitation of Argonaute, co-immunoprecipitated mRNA transcripts were isolated and identified by high-throughput sequencing. Argonaute binding sites (i.e., peaks) that were enriched in cells transfected with miR-194 compared to control-transfected cells were identified using MACS2 (Zhang et al., 2008), yielding 7,772 peaks associated with 3,326 genes (Table S1). An example peak at the *ZBTB10* gene is shown in Figure 1A. Highlighting the robustness of the data, the vast majority (94%) of peaks were located within genes, most commonly in exons, 3′ UTRs and introns (Figure 1B). Furthermore, unbiased *de novo* motif analysis revealed that the most strongly enriched sequence within the peaks was a miR-194 seed recognition site (Table S2), which was concentrated within the centers of peaks (Figure 1C).

miRNAs typically reduce the levels of their target mRNAs (Eichhorn et al., 2014; Guo et al., 2010; Selbach et al., 2008). Therefore, we conducted RNA sequencing (RNA-seq) of 22Rv1 cells transfected with miR-194 mimic or a control. miR-194 elicited significant changes to the transcriptome, causing downregulation of 2,626 and upregulation of 2,485 mRNA transcripts (Figure 1D). Integration of the RNA-seq and Ago-HITS-CLIP datasets revealed a strong bias toward downregulation of mRNAs with Ago-HITS-CLIP peaks in 3′ UTRs, whereas mRNAs with peaks in coding regions were less strongly biased toward downregulation and those with peaks in introns were collectively unchanged (Figure 1E; Figure S1A). Transcripts with 3′ UTR peaks containing miR-194 seed recognition sequences tended to be more robustly downregulated than those lacking such sequences (Figure 1F; Figure S1B). These findings are consistent with previous studies demonstrating that 3′ UTRs are the key sequences through which miRNAs exert their activity (Lewis et al., 2005; Chi et al., 2009).

To further prioritize putative miR-194 target genes, we used Exon-Intron Split Analysis (EISA), a bioinformatic technique that separates transcriptional and post-transcriptional effects

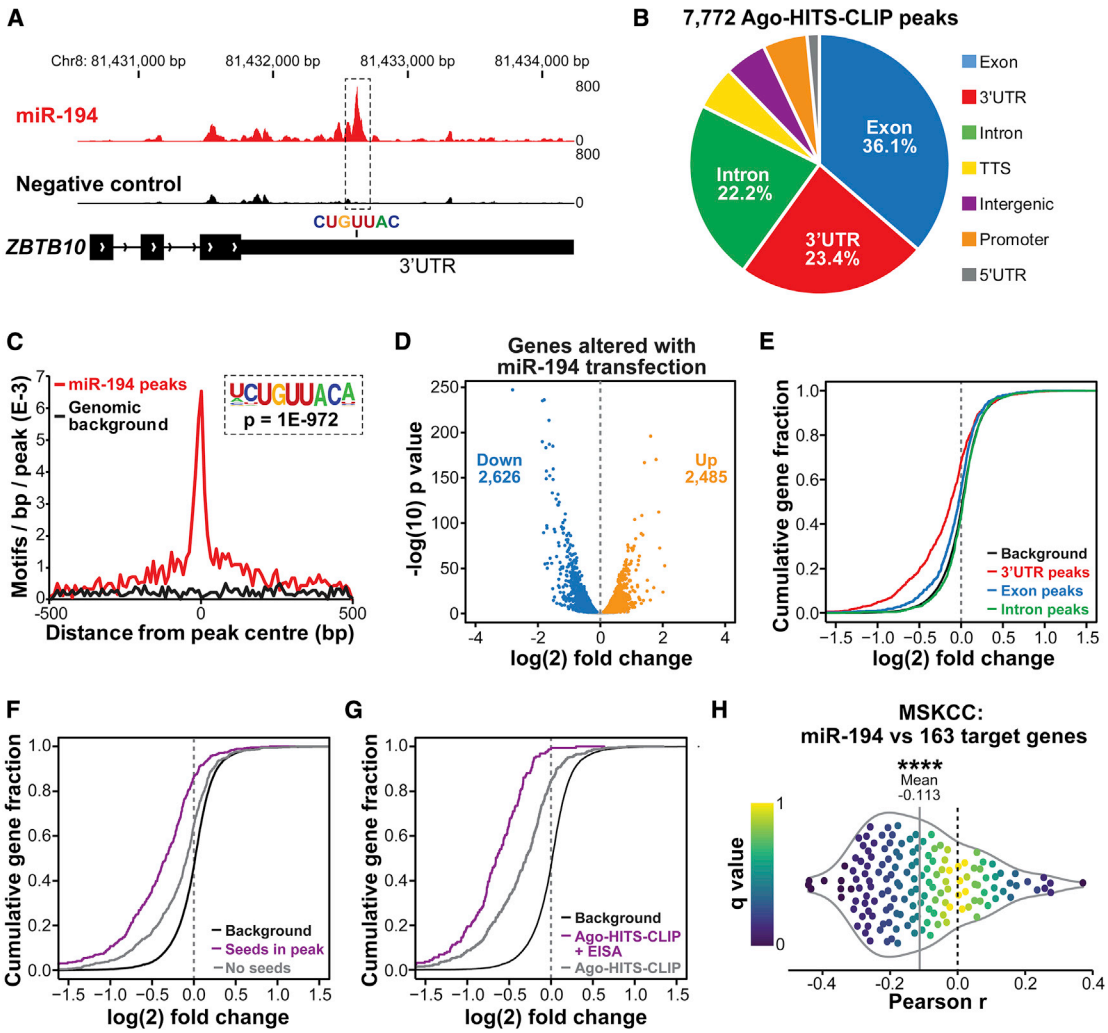

Figure 1. Identification of a miR-194 "Targetome" in Prostate Cancer

(A) Example of an Ago-HITS-CLIP peak with a miR-194 seed recognition sequence in the *ZBTB10* gene. Genome tracks depict the average read density of all replicates for each treatment condition (i.e., cells transfected with miR-194 [red] or a scrambled control [black]).

(B) Distribution of 7,772 Ago-HITS-CLIP peaks mapped to their genomic regions.

(C) Distribution of miR-194 recognition sequences within Ago-HIT-CLIP peaks. Background represents occurrence of the motif on the opposite strand of the peak.

(D) Volcano plot showing expression of genes altered by miR-194 transfection in 22RV1 cells. Blue dots indicate significantly downregulated genes, and orange dots indicate significantly upregulated genes (false discovery rate [FDR], ≤ 0.05).

(E) Cumulative distribution of log2 fold change for genes containing peaks in the 3′ UTR, CDS, and introns compared to a background of all genes with no peaks.

(F) Cumulative distribution of log2 fold change for genes with a 3′ UTR Ago-HITS-CLIP peak containing miR-194 seed matches or no seed matches in peaks compared to a background of all genes with no peaks.

(G) Cumulative distribution of log2 fold change for all genes with a 3′ UTR Ago-HITS-CLIP peak containing a miR-194 seed match (Ago-HITS-CLIP) or both a 3′ UTR peak with miR-194 seed match and downregulation at the post-transcriptional level (Ago-HITS-CLIP + EISA).

(H) Correlations between miR-194 expression and its targetome in 72 primary and metastatic prostate cancers (MSKCC cohort; Taylor et al., 2010). For each target identified, the Pearson correlation coefficient and its q value was calculated and plotted as −log q (on y axis) versus correlation coefficient (on x axis). To indicate the bias toward negative correlations, the mean correlation coefficient is indicated by a vertical black line. p value was determined using a one-sided t test (****$p < 0.0001$).

See also Figure S1 and Tables S1, S2, and S3.

by evaluating whether RNA-seq reads map to exons or introns (Gaidatzis et al., 2015). The quality and number of predicted 3′UTR miR-194 target sites were strongly associated with genes downregulated at a post-transcriptional but not a transcriptional level (Figure S1C), indicating that EISA can differentiate between direct miR-194 targets and downstream changes to the transcriptome. Moreover, transcripts exhibiting post-transcriptional but not transcriptional alterations exhibited stronger downregulation by miR-194 than all transcripts containing Ago-HITS-CLIP peaks (Figure 1G).

With these observations in mind, we applied a filtering strategy whereby transcripts with 3′ UTR Ago-HITS-CLIP peaks containing seed recognition sequences and predicted to be downregulated post-transcriptionally were included in a final, high-confidence 163-gene miR-194 "targetome." To assess the biological relevance of the targetome, its correlation with miR-194 levels was evaluated in 65 primary tumors and 7 metastases from a public prostate cancer transcriptomic resource (Taylor et al., 2010). We observed a distinct bias toward inverse correlation between miR-194 and its target genes (Figure 1H), supporting the notion that our experimental strategy integrating biochemistry, molecular biology, and bioinformatics (i.e., Ago-HITS-CLIP, RNA-seq, and EISA) identified bona fide targets.

miR-194 Expression and Activity Are Negatively Correlated with AR Signaling

Gene Ontology analysis of the miR-194 targetome revealed enrichment for genes associated with cytoskeletal remodeling, cell adhesion, and cell motility (Table S3), consistent with the ability of miR-194 to induce an EMT and enhance PCa cell migration and invasion (Das et al., 2017). To evaluate the targetome more specifically in clinical prostate cancer, we used single sample gene set enrichment analysis (ssGSEA) of our high-confidence targetome to generate miR-194 activity scores in clinical cohorts, which were then compared to activity scores generated for the "hallmark" biological gene sets derived from the same cohorts (Liberzon et al., 2015). Because miRNAs repress expression of their target genes, miR-194 activity was defined as the inverse value of ssGSEA scores for the miR-194 targetome. One striking finding was that miR-194 activity was strongly inversely correlated with AR signaling across all cohorts examined (Figure 2A; Table S4). This observation was validated using a more refined set of AR target genes (Figure 2B) recently generated by Sowalsky and colleagues (Sowalsky et al., 2018).

The strong negative association between miR-194 and AR activity led us to examine whether the miR-194 targetome was enriched for AR target genes, but there was only a limited overlap between these gene sets (Figure 2C). Moreover, our Ago-HITS-CLIP and transcriptomic data indicated that miR-194 does not target the *AR* transcript (Figures S2A and S2B). An alternative (and/or additional) explanation for this inverse relationship could be that AR regulates the expression of miR-194. Indeed, levels of miR-194 in the androgen-sensitive LNCaP model were decreased by the potent androgen DHT and increased by the AR antagonist enzalutamide (Figure 2D). In accordance with these findings, extended culture of cells under androgen-depleted conditions led to upregulation of miR-194 (Figure 2E). Collectively, these data reveal that AR represses expression of miR-194, which (at least partly) explains the negative association between these factors in clinical prostate cancer.

AR is a transcription factor that binds to regulatory elements within enhancers and, less commonly, promoters of its target genes (Wang et al., 2009). To gauge whether miR-194 expression is directly regulated by AR, we first interrogated publicly available AR chromatin immunoprecipitation sequencing (ChIP-seq) data, which revealed no evidence for association of AR with regulatory elements proximal to the *MIR194* genes (Figure S2C). Moreover, the kinetic response to miR-194 regulation by DHT and enzalutamide is in the order of days, rather than the hours expected for direct transcriptional regulation (Figure S2D). Collectively, these data support an indirect mechanism by which AR represses miR-194 expression in PCa.

miR-194 Activity and Expression Are Elevated in NEPC

NEPC is associated with loss of canonical AR activity (Davies et al., 2018). Given the inverse relationship between miR-194 and AR, we therefore hypothesized that its activity would be elevated in clinical NEPC. Indeed, miR-194 activity (estimated by ssGSEA) was significantly higher in NEPC than in CRPC-Adeno tumors in clinical samples (Figure 3A) and patient-derived xenograft (PDX) models of PCa (Figure S3). Moreover, miR-194 activity was correlated with established NEPC gene sets (Figure 3B).

We next examined whether miR-194 itself was overexpressed in NEPC. In the absence of miRNA expression data from clinical samples, we turned to a panel of 13 PDXs established through the Melbourne Urological Research Alliance (MURAL), of which 6 have features of NEPC (Lawrence et al., 2018). Importantly, miR-194 expression was higher in the NEPC than in the AR-positive adenocarcinoma PDXs (Figure 3C), further demonstrating its association with this disease subtype.

Loss of AR expression and/or activity during the transition to NEPC feasibly explains increased miR-194 expression in this disease state. However, because we have also noted elevated miR-194 expression and activity in metastases and "poor outcome" primary tumors (Selth et al., 2013), we speculated that other alterations may underlie dysregulation of miR-194 in PCa. miR-194 is encoded by two separate genes on chromosomes 1 and 11; the *MIR194-1* gene clusters with *MIR215* within intron 12 of *IARS2* on chromosome 1, and the *MIR194-2* gene clusters with *MIR192* approximately 3 kb downstream of *ATG2A* on chromosome 11. By interrogating clinical genomic datasets, we found that *MIR194-1/IARS2* and *MIR194-2/ATG2A* are more frequently gained/amplified in metastatic compared to primary PCa and in NEPC compared to CRPC-Adeno (Figure 3D). Importantly, gain/amplification of these loci were associated with elevated levels of miR-194 (Figure 3E). Collectively, these data suggest that in addition to loss of AR expression or activity, *MIR194* copy number gain can result in increased miR-194 expression in aggressive prostate tumors and NEPC.

miR-194 Promotes the Emergence of NE Features in Prostate Cancer

To determine whether miR-194 can directly influence the emergence of an NE-like state, we examined the phenotypic response of adenocarcinoma PCa cells to transfection with a miR-194 mimic. Exogenous miR-194 upregulated NE marker genes (Figure 4A) and increased neurite length (Figure 4B) in LNCaP cells, an effect that was recapitulated in the 22Rv1 cell line model (Figures 4A and 4B; Figure S4).

The ability of miR-194 to enhance NE transdifferentiation was further tested using a locked nucleic acid (LNA) inhibitor that specifically inhibits the activity of this oncogenic miRNA. In these experiments, we exploited the fact that the LNCaP model can be

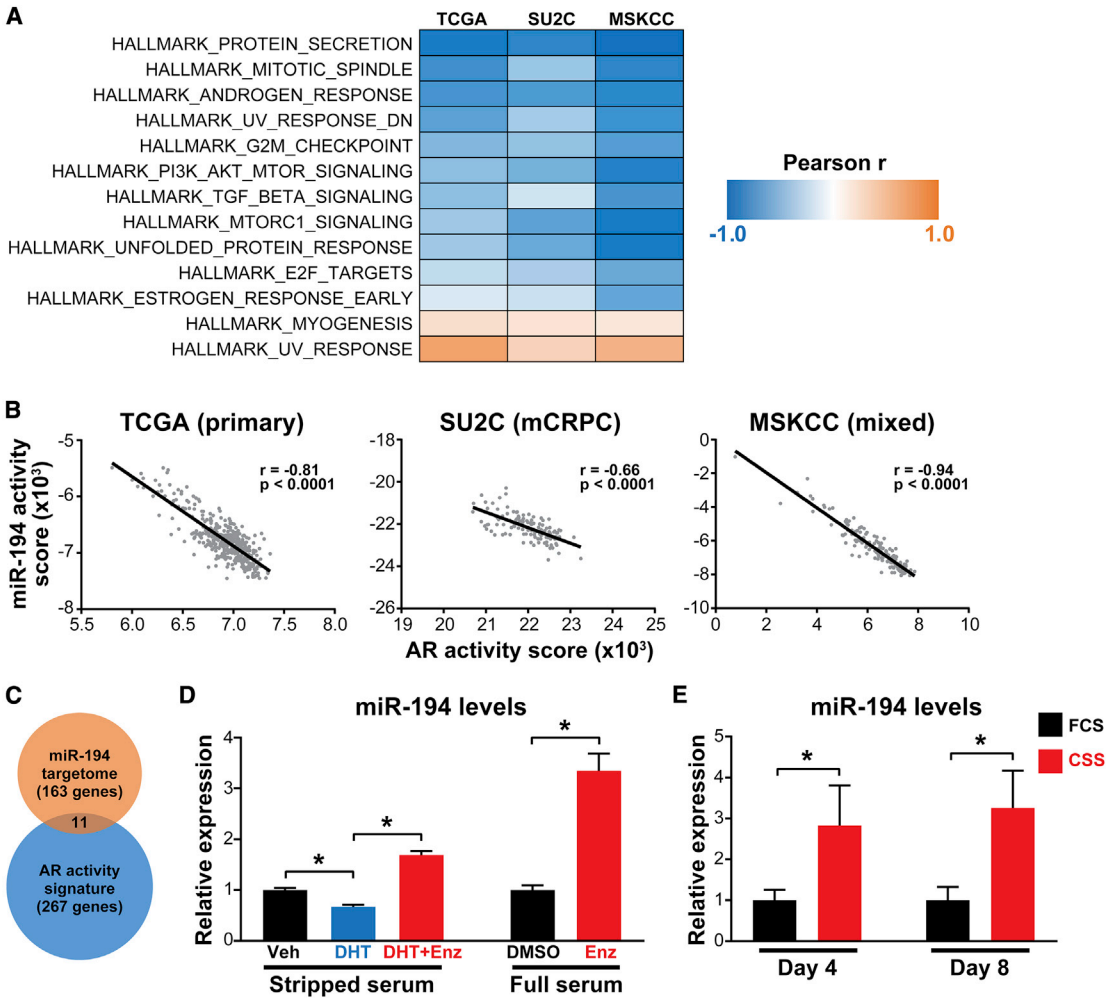

Figure 2. miR-194 Expression Is Suppressed by AR Signaling

(A) Correlation of miR-194 activity score with activity scores of "hallmark" biological gene sets in the TCGA, SU2C, and MSKCC cohorts. p and r values were determined using Pearson's correlation tests. Only gene sets that were significantly correlated ($p < 0.05$) in all three cohorts are shown in the heatmap.

(B) miR-194 activity is inversely correlated with AR activity in primary prostate cancer (TCGA cohort, left; Cancer Genome Atlas Research Network, 2015), metastatic prostate cancer (SU2C cohort, center; Robinson et al., 2015), and a cohort comprising both primary and metastatic prostate cancer (MSKCC cohort, right; Taylor et al., 2010). p and r values were determined using Pearson's correlation tests.

(C) Overlap between the miR-194 targetome and an AR target gene set (Sowalsky et al., 2018).

(D) Relative miR-194 expression in LNCaP cells treated with the androgen DHT and AR antagonist enzalutamide (Enz). Cells grown in stripped serum were treated with vehicle control (Veh) or 10 nM DHT in the presence or absence of 10 μM Enz for 48 h. Cells grown in full serum were treated with vehicle (DMSO) or 10 μM Enz for 48 h. Expression of miR-194 was normalized to the reference small RNA U6. p values were determined using unpaired two-sided t tests (*$p < 0.05$).

(E) Relative miR-194 expression in LNCaP cells grown in fetal calf serum (FCS) or charcoal stripped serum (CSS) for 4 or 8 days. Expression of miR-194 was normalized to the reference small RNA U6. p value was determined using an unpaired two-sided t test (*$p < 0.05$).

Data shown in (D) and (E) are representative of at least two independent experiments of three replicates each; error bars represent SEM. See also Figure S2 and Table S4.

transdifferentiated from adenocarcinoma-like to NE-like cells by androgen deprivation (Shen et al., 1997). As expected, growth of cells in charcoal-stripped serum (CSS) to deplete steroid hormones resulted in upregulation of NE markers *ENO2* (encoding neuron-specific enolase) and *SYP* (encoding synaptophysin) and increased the length of neurite-like extensions (Figures 4C and 4D). Importantly, the miR-194 LNA inhibitor effectively blocked this transdifferentiation (Figures 4C and 4D). Collectively, these data reveal that miR-194 can drive the acquisition of NE features, which corresponds with its increased activity in clinical NEPC.

NEPC is associated with a reduced dependence on AR signaling and, hence, resistance to AR-targeted therapies. Therefore, we speculated that miR-194 could alter the responsiveness of PCa cells to modulators of the AR signaling axis. To test this hypothesis, we generated LNCaP cells that stably overexpressed miR-194 (LNCaP-194; Figure 4E). Overexpression of miR-194 conferred a growth advantage in the absence of androgens (CSS; Figure 4F)

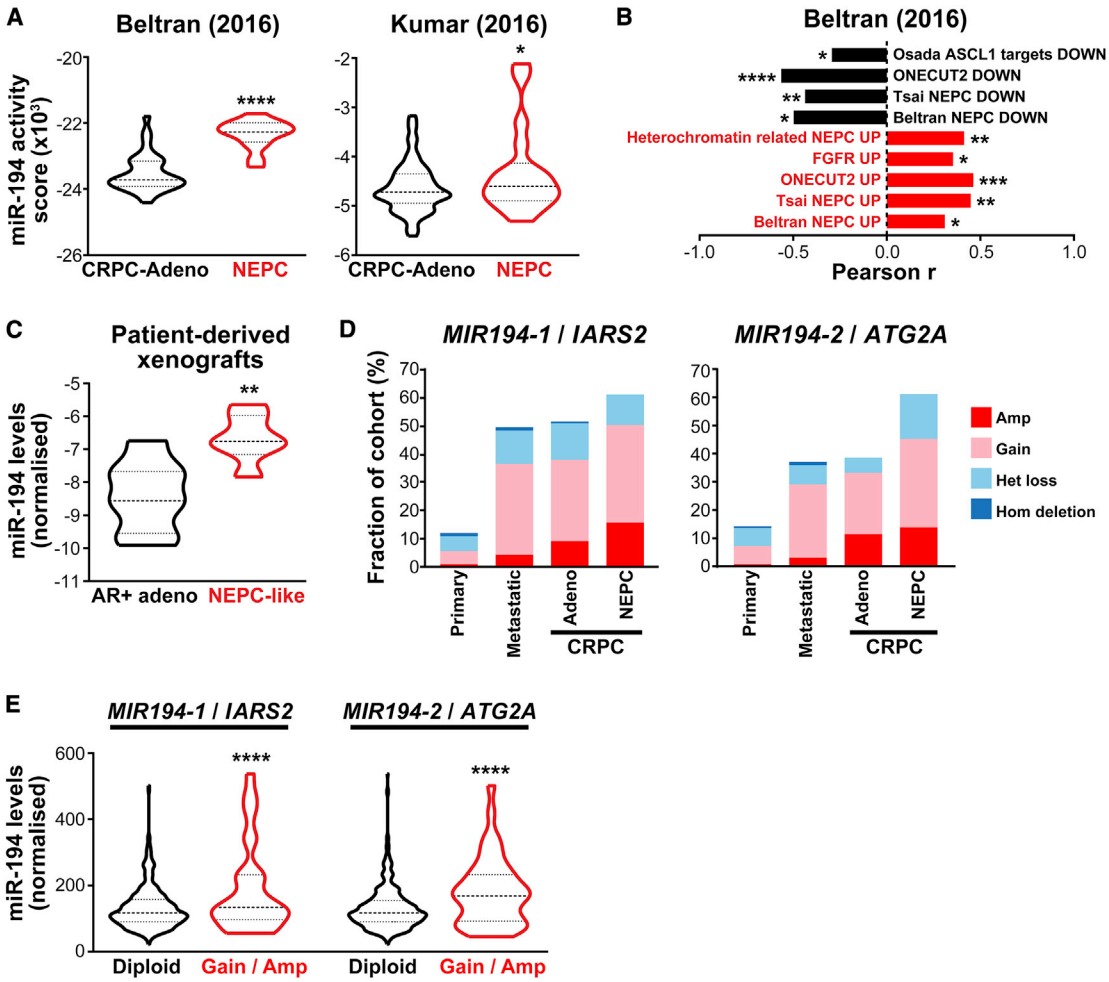

Figure 3. miR-194 Activity and Expression Are Elevated in Neuroendocrine Prostate Cancer

(A) miR-194 activity is higher in NEPC than in adenocarcinoma CRPC (CRPC-Adeno) in two distinct cohorts (Beltran et al., 2016; Kumar et al., 2016). Dashed middle line, median; dotted lines above and below, upper and lower quartiles. p values were determined using unpaired two-sided t tests (*p < 0.05; ****p < 0.0001).

(B) Correlation between miR-194 activity and published NEPC-associated gene signatures (Beltran et al., 2016; Ci et al., 2018; Delpuech et al., 2016; Guo et al., 2019; Tsai et al., 2017; Osada et al., 2008). p and r values were determined using Pearson's correlation tests (*p < 0.05; **p < 0.01; ***p < 0.001; ****p < 0.0001).

(C) Expression of miR-194 is higher in NEPC PDXs (n = 6) than in PDXs derived from AR-positive adenocarcinoma (n = 7) tumors. Expression of miR-194 was normalized to two reference small RNAs (U6 and RNU44). Dashed middle line, median; dotted lines above and below, upper and lower quartiles. p value was determined using an unpaired two-sided t test (**p < 0.01).

(D) *MIR194-1/IARS2* and *MIR194-2/ATG2A* are more frequently gained/amplified in metastatic compared to primary PCa and in NEPC compared to CRPC-Adeno. Copy number data were combined from multiple clinical cohorts (Armenia et al., 2018; Abida et al., 2019; Beltran et al., 2016; Grasso et al., 2012; Taylor et al., 2010).

(E) Expression of miR-194 is higher in primary prostate tumors with *MIR194-1/IARS2* or *MIR194-2/ATG2A* copy number gain or amplification than in tumors with no change in copy number (diploid). Data are from the TCGA cohort. Dashed middle line, median; dotted lines above and below, upper and lower quartiles. p values were determined using unpaired two-sided t tests. (****p < 0.0001).

See also Figure S3.

and in full serum supplemented with the AR antagonist enzalutamide (Figure 4G). These findings suggest that the phenotypic changes elicited by miR-194 could have clinically relevant consequences in relation to resistance to AR-targeted therapies.

miR-194 Targets FOXA1 and Activates ERK Signaling

To understand at a mechanistic level how miR-194 promotes PCa NE phenotypes, we searched the targetome for genes with a known role in PCa progression. Of particular interest was Forkhead box protein A1 (FOXA1), a transcription factor with a critical role in maintaining the prostatic epithelial lineage (Bernardo and Keri, 2012). Consistent with this function, a study demonstrated that loss of FOXA1 leads to NE differentiation in prostate cancer (Kim et al., 2017). Multiple miR-194 Ago-HITS-CLIP peaks were found within the *FOXA1* 3′ UTR, of which one contains a perfect 7-mer seed match (Figure 5A). We confirmed

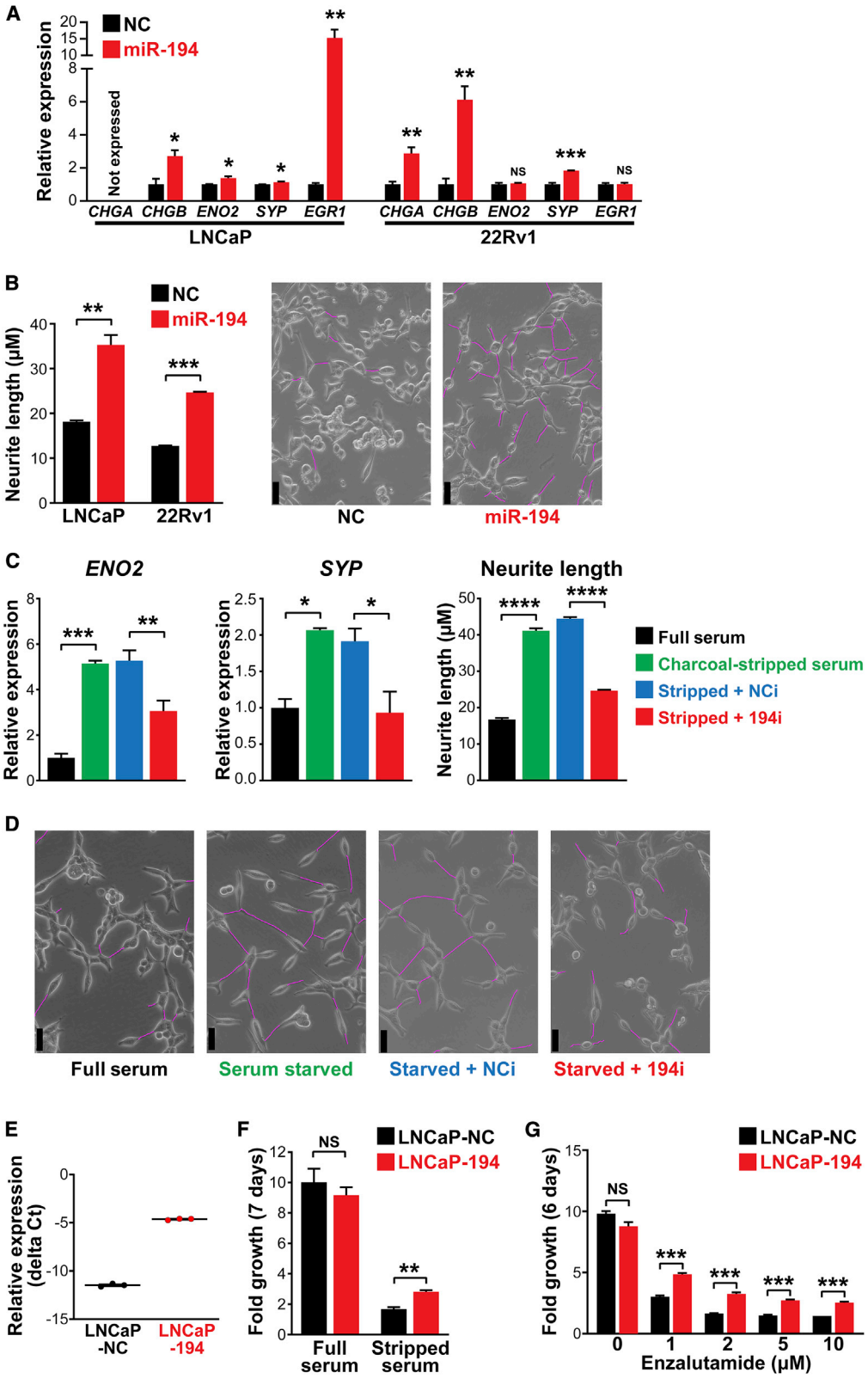

(legend on next page)

that miR-194 decreased the levels of *FOXA1* mRNA and FOXA1 protein in the LNCaP and 22Rv1 models (Figures 5B and 5C). Conversely, the miR-194 LNA inhibitor increased levels of FOXA1 in a model of PCa, MR42D, that possesses NE features (Figure 5B; Bishop et al., 2017). FOXA1 shares a high degree of homology with its paralogs FOXA2 and FOXA3 (Li et al., 2017a). However, miR-194 Ago-HITS-CLIP peaks were not evident within either of these genes, and they were not expressed at appreciable levels in PCa cells (Figures S5A–SC). Supporting the relevance of FOXA1 as a downstream target of miR-194, genes upregulated by FOXA1 tended to be repressed in cells transfected with miR-194 (Figure S5D). Moreover, the activity of FOXA1 and miR-194 is inversely correlated in clinical PCa (NEPC and primary PCa; Figure 5D). Collectively, these findings reveal FOXA1 as a direct target of miR-194 with functional relevance in PCa.

To elucidate functional consequences of FOXA1 downregulation by miR-194, we used ChIP-seq to measure the genome-wide DNA binding pattern of FOXA1. miR-194 altered FOXA1 binding at 32,963 sites, with the predominant effect being FOXA1 loss (20,526 sites) (Figure 5E). Importantly, at binding sites associated with FOXA1-regulated genes, miR-194 caused an overall decrease of FOXA1 binding (Figure 5F). This included FOXA1-repressed genes that can promote a NE phenotype in prostate cancer, including the chemokine *IL8* and the EMT transcription factors *SNAI2* (Slug) and *ZEB1* (Kim et al., 2017; Jin et al., 2013; Li et al., 2014); miR-194 caused loss of FOXA1 binding proximal to these genes (Figure 5E), concomitant with increased mRNA expression (Figure 5G). A downstream consequence of increased IL-8 expression in response to FOXA1 loss is activation of the mitogen-activated protein kinase (MAPK)/ERK pathway (Kim et al., 2017); moreover, positive feedback loops between Slug/ZEB1 and ERK exist in multiple oncogenic contexts (Drápela et al., 2020; Jiang et al., 2014; Smith et al., 2014). Considering these links and the known importance of ERK in NEPC (Kim et al., 2002; Bluemn et al., 2017), we further examined ERK activation in the context of miR-194. Transfection of PCa cells with miR-194 resulted in enhanced MAPK/ERK pathway activity (Figure S5E) and elevated levels of active (phosphorylated) ERK in two distinct models of androgen-driven PCa (Figure 5H), whereas the miR-194 LNA inhibitor decreased expression of ERK pathway genes in models with NE features (Figure 5I). Moreover, miR-194 activity was positively correlated with ERK gene signatures in clinical NEPC (Figures 5G and S5F). Collectively, these data reveal downstream consequences of FOXA1 targeting by miR-194 associated with enhanced phenotypic plasticity and tumor aggressiveness.

Co-targeting of Multiple NEPC-Related Factors by miR-194

To further investigate the relevance of FOXA1 as a target by which miR-194 stimulates epithelial-NE transdifferentiation in PCa, we engineered LNCaP cells to stably express an inducible form of FOXA1 lacking the 3′ UTR (Figure 6A). Expression of this "non-targetable" FOXA1 partially rescued the effects of exogenous miR-194, demonstrated by a moderate reduction of neurite length (Figure 6B) and suppression of miR-194-induced *SNAI2* (Figure 6C), but had no effect on *IL8* and *ENO2* (Figure 6C). Transient expression of non-targetable FOXA1 in another PCa model, 22Rv1, also rescued miR-194-induced neurite extensions (Figure 6B). A different set of genes were measured in 22Rv1 cells based on expression (i.e., *IL8* is not detectable in 22Rv1 cells) and robustness of response to miR-194 in earlier experiments (refer to Figure 4A); FOXA1 partially rescued *CHGA* expression but had no effect on *CHGB* or *SNAI2* (Figure 6C). Collectively, these findings support a role for FOXA1 in mediating some, but not all, effects of miR-194 in a context-dependent manner.

Because miR-194 targets >100 genes in PCa cells (Figure 1), the failure of FOXA1 to completely rescue the miR-194-induced phenotypes is not unexpected and led us to consider other targets in relation to NEPC. Comprehensive literature-based annotation of the miR-194 targetome genes revealed at least 10 factors that can reportedly suppress NE-related plasticity in PCa, including AHR, ARHGAP1, ARL6IP5, ATXN1, FBXW2, FOXA1, THBS1, TRAF6, TRIM36, and ZBTB10 (Figure 6D). We validated downregulation of a subset of these genes using qRT-PCR (Figure S6). These data suggest that miR-194 mediates its pro-plasticity effects in PCa by network-level gene regulation, of which FOXA1 is one component.

Figure 4. miR-194 Promotes Prostate Cancer Transdifferentiation

(A) Expression of NEPC marker genes is upregulated in response to transfection of a miR-194 mimic for 72 h in LNCaP and 22RV1 cells. Gene expression was normalized to GAPDH. Expression for the negative control (NC) was set to 1, and error bars are SEM.

(B) Neurite length is increased in response to transfection of a miR-194 mimic for 72 h in LNCaP and 22RV1 cells. Expression for NC was set to 1. p values were determined using unpaired two-sided t tests (**$p < 0.01$). Representative phase contrast images (on the right) are of LNCaP cells transfected with miR-194 mimic or NC. Neurite outgrowths are traced on images in magenta. Scale bars, 25 μm.

(C) A miR-194 inhibitor (194i) blocks neuroendocrine transdifferentiation of LNCaP cells mediated by androgen deprivation, as determined by expression of neuron-specific enolase (*ENO2*), synaptophysin (*SYP*), and changes in neurite length at 96 h post-transfection. Gene expression was normalized to GAPDH. Gene expression or neurite length for cells grown in full serum were set to 1. p values were determined using ANOVA (*$p < 0.05$; **$p < 0.01$; ***$p < 0.001$; ****$p < 0.0001$).

(D) Representative phase contrast images of LNCaP cells grown under full or stripped serum conditions with or without a miR-194 inhibitor (194i) or NC inhibitor (NCi). Neurite outgrowths are traced in magenta. Scale bars, 25 μm.

(E) Relative expression of miR-194 in LNCaP cells stably expressing miR-194 (LNCaP-194) or a scrambled control (LNCaP-NC).

(F) Growth of LNCaP-194 and LNCaP-NC cells under full serum or charcoal-stripped (androgen-deprived) conditions. Fold growth over a period of 7 days was calculated relative to the number of cells present at day 0. p values were determined using unpaired two-sided t tests (**$p < 0.01$).

(G) Growth of LNCaP-194 and LNCaP-NC cells in response to Enz. Fold growth over a period of 6 days was calculated relative to the number of cells present at day 0. Error bars are SEM; p values were determined using unpaired two-sided t tests (***$p < 0.001$).

Data shown in (A)–(C), (F), and (G) are representative of at least two independent experiments of three replicates each; error bars represent SEM. See also Figure S4.

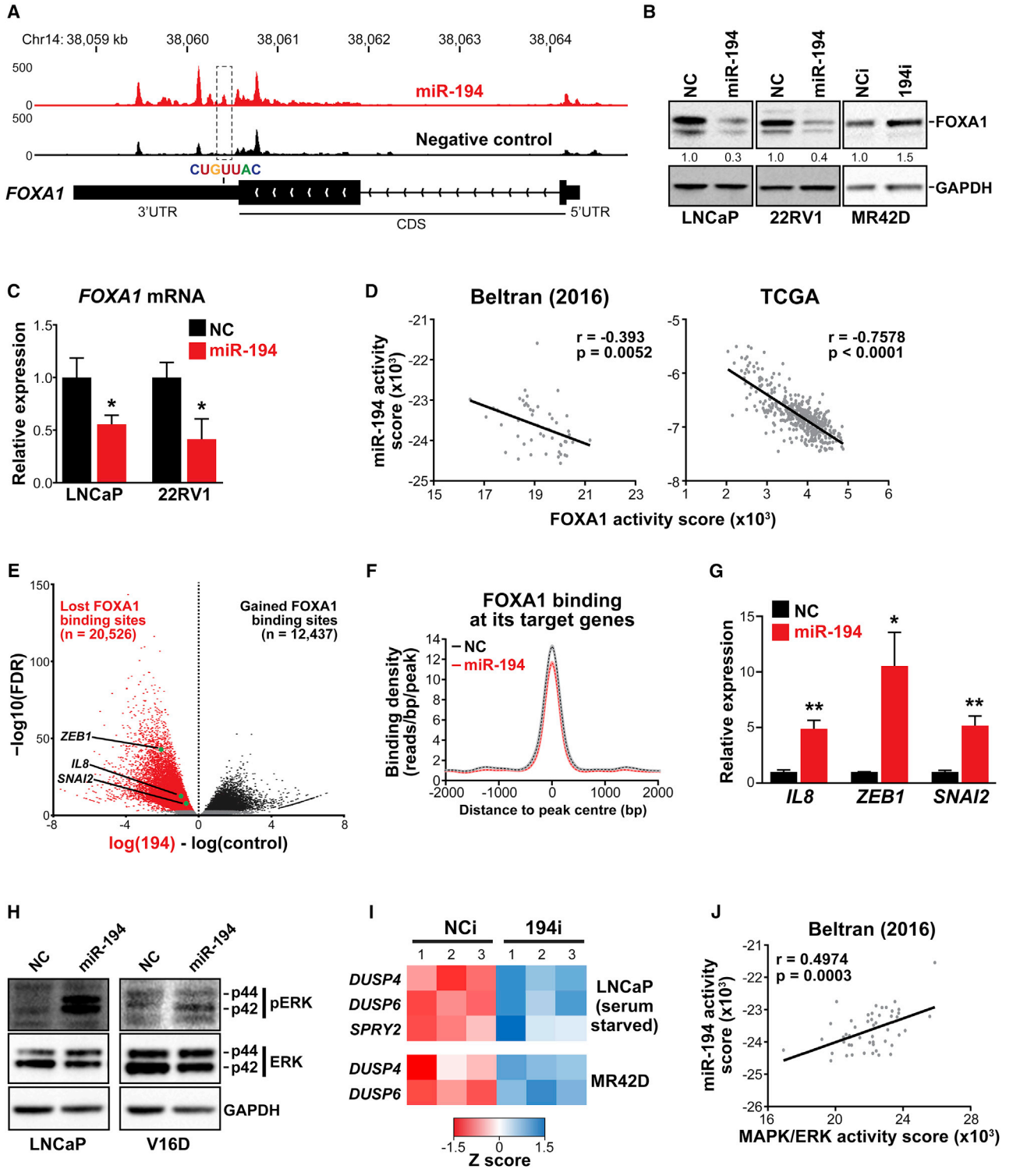

Figure 5. miR-194 Targets FOXA1 and Activates the MAPK/ERK Pathway

(A) Ago-HITS-CLIP peaks (including one indicated with a miR-194 seed recognition) sequence in the *FOXA1* gene. Genome tracks depict the average read density of all replicates for each treatment condition (i.e., cells transfected with miR-194 [red] or a scrambled control [black]).

(B) Western blot showing FOXA1 protein levels following transfection of a miR-194 mimic or negative control (NC) for 48 h (22RV1 and LNCaP cells) or following transfection of a miR-194 inhibitor (miR-194i) or NCi for 72 h (MR42D cells).

(legend continued on next page)

Targeting miR-194 Suppresses the Growth of Prostate Cancer with NE Features

Although miR-194 mediates the acquisition of an NE-like phenotype in prostate cancer, whether it represents a therapeutic target in this disease context is unclear. To investigate this possibility, we measured the growth of PCa cells treated with the miR-194 LNA inhibitor. Interestingly, the growth of all 4 cell line models tested could be suppressed by the inhibitor, but the models with NE features (PC3 and LNCaP-MR42D) were more sensitive than those with a more typical adenocarcinoma phenotype (LNCaP and LNCaP-MR49F) (Figure 7A). The miR-194 inhibitor was cytotoxic, as revealed by cell viability assays (Figure 7B) and by counting dead cells (Figure 7C).

To examine the potential of targeting miR-194 in a more clinically relevant setting, we turned to patient-derived CRPC organoids recently described by our team (Lawrence et al., 2018). Models 201.1 and 201.2 were derived from dura and lung metastases, respectively, from a patient who died after receiving second-generation AR-targeted therapies (enzalutamide and abiraterone) and chemotherapies (docetaxel and cabazitaxel) (Lawrence et al., 2018). 201.1 is a model of PSA-positive adenocarcinoma that expresses a mutated form of the AR (C687Y and T878A) that mediates resistance to enzalutamide. In contrast, 201.2 has no AR or PSA expression but exhibits high expression of a NE gene signature, focal staining of CD56, and concurrent genomic loss of *TP53*, *PTEN*, and *RB1* (Lawrence et al., 2018). Representative immunohistochemistry (IHC) images of the expression of various markers in each model are shown in Figure 7D. As expected, miR-194 levels were higher in model 201.2 than in model 201.1 (Figure 7E). The effect of the miR-194 LNA inhibitor on the growth of these two patient-derived models was evaluated by measuring organoid forming efficiency (OFE) and cell viability. Both models exhibited reduced OFE and cell viability in response to transfection with the inhibitor (Figures 7F and 7G). However, similar to the cell lines, the AR null, NEPC-like 201.2 model was more sensitive to miR-194 inhibition than the adenocarcinoma-like 201.1 model (Figures 7F and 7G). Collectively, these findings—in both traditional cell lines and contemporary patient-derived models—provide evidence that targeting miR-194 has potential as a therapy for prostate cancer with NE features.

DISCUSSION

Epigenetic and transcriptional alterations are known to mediate prostate cancer cell plasticity during adenocarcinoma-NE transdifferentiation. Most drivers of these alterations identified to date are transcription factors and chromatin modifiers, such as SOX2 (Ku et al., 2017; Mu et al., 2017), EZH2 (Ku et al., 2017), REST (Li et al., 2017c), BRN2 (Bishop et al., 2017), and FOXA2 (Qi et al., 2010). By identifying miR-194 as a mediator of this transdifferentiation, our work reveals that post-transcriptional gene regulation by miRNAs is another mechanism by which transcriptional networks are altered during progression to NEPC.

Our study suggests that miR-194 is elevated in NEPC by two non-mutually exclusive mechanisms. First, by evaluating PCa cells treated with androgens and anti-androgens, we found that miR-194 is negatively regulated by the AR signaling axis. Interrogation of published AR cistromic data and analysis of the kinetics of androgen-mediated downregulation of miR-194 supported a mechanism whereby AR indirectly inhibits miR-194 expression. One possibility is that the transcription factor GATA2 serves as an intermediary: expression of GATA2 is known to be downregulated by AR (He et al., 2014), and we previously demonstrated that GATA2 enhances the levels of miR-194 (Das et al., 2017). Future studies should investigate the role of this putative pathway in NEPC, particularly because GATA2 is known to promote PCa metastasis and drug resistance (Vidal et al., 2015). Second, we found that gain or amplification of genomic regions encompassing the *MIR194* genes is another mechanism that can result in elevated expression of miR-194 in aggressive forms of prostate cancer, including NEPC. miR-194 is unusual in that it is encoded by 2 genes (*MIR194-1* and *MIR194-2*), and the observation that both are frequently gained further supports the relevance of this miRNA in disease progression.

Using an integrative approach that exploited cutting-edge biochemical (Ago-HITS-CLIP), molecular (RNA-seq), and bioinformatics (EISA) techniques, we identified ~160 genes that miR-194 putatively targets in PCa. Of note, gene signatures enriched in this targetome include those involved in cell movement, cytoskeletal organization (including axon guidance), and focal adhesion. We propose that dysregulation of these networks by elevated miR-194 during PCa progression promotes EMT

(C) Expression of *FOXA1* mRNA, as determined by qRT-PCR, following transfection of miR-194 mimic or NC for 48 h in 22RV1 and LNCaP cells. Gene expression was normalized to GAPDH. Expression for NC was set to 1. p values were determined using unpaired two-sided t tests (*$p < 0.05$).
(D) FOXA1 activity is negatively correlated with miR-194 activity in clinical cohorts (Beltran et al., 2016; Cancer Genome Atlas Research Network, 2015). p and r values were determined using Pearson's correlation tests.
(E) Volcano plot showing gained (red) or lost (black) FOXA1 binding following transfection of miR-194 in LNCaP cells. Differentially bound sites were called using Diffbind.
(F) Binding density of FOXA1 at target sites in cells transfected with miR-194 (red) or negative control (NC) (black). Shaded regions are ± SEM.
(G) Expression of *IL8*, *ZEB1*, and *SNAIL2* in response to miR-194 transfection for 72 h in LNCaP cells. Gene expression was normalized to GAPDH. Expression for NC was set to 1. p values were determined using unpaired two-sided t tests (*$p < 0.05$; **$p < 0.01$).
(H) Western blot showing ERK and phospho-ERK protein levels in LNCaP and V16D cells transfected for 72 h with a miR-194 mimic or negative control (NC).
(I) Expression of markers of *ERK* activation, as determined by qRT-PCR, following transfection of miR-194 inhibitor (miR-194i) or NCi in serum-starved LNCaP cells (genes measured at 96 h post-transfection) or MR42D cells (genes measured at 72 h post-transfection). Gene expression was normalized to GAPDH. Data are represented as *Z* scores.
(J) MAPK/ERK activity is positively correlated with miR-194 activity in a clinical cohort comprised of NEPC and CRPC-Adeno samples (Beltran et al., 2016). p and r values were determined using a Pearson's correlation test.
Data shown in (C), (G), and (I) are representative of at least two independent experiments of three replicates each; error bars represent SEM. See also Figure S5.

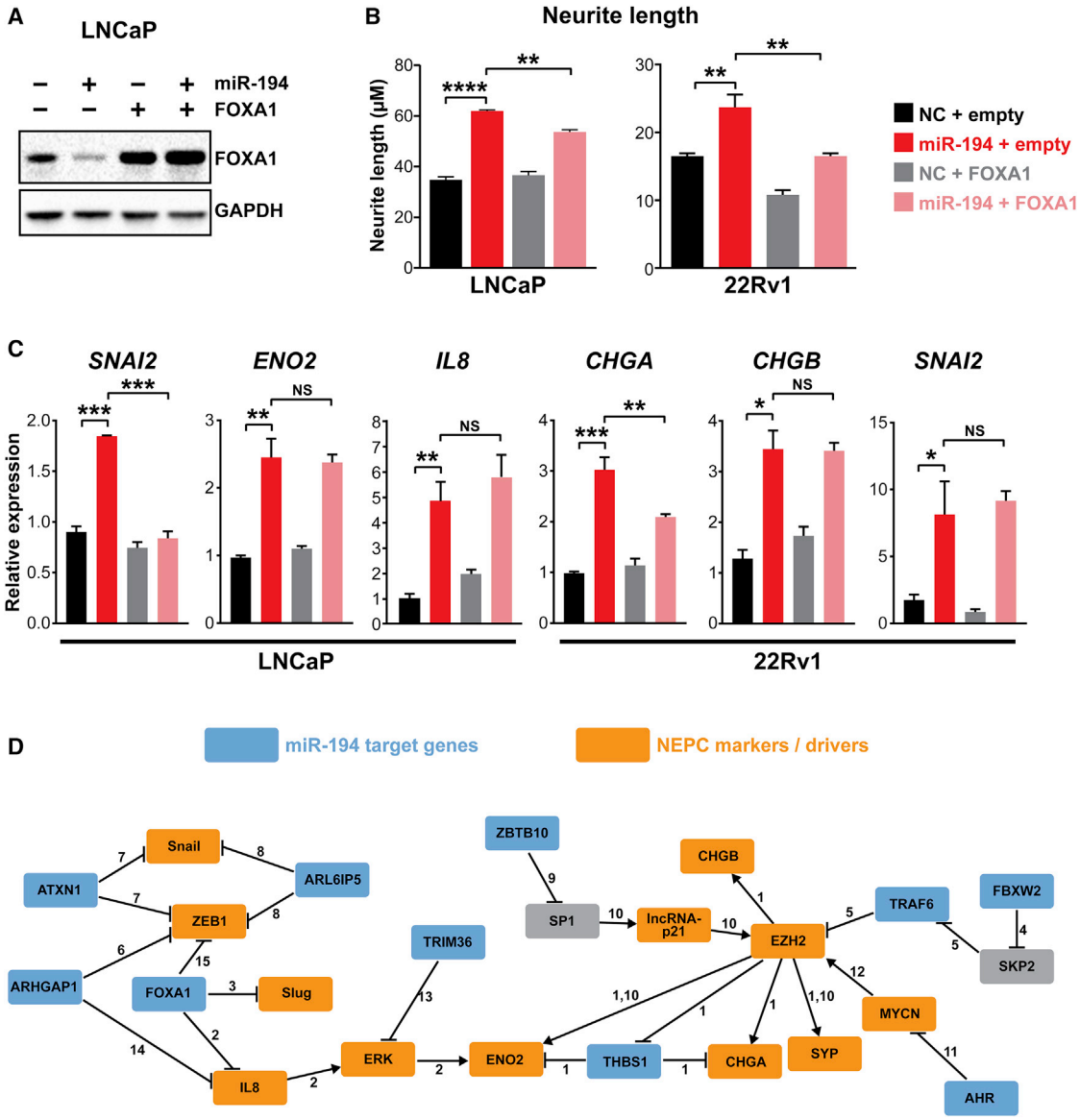

Figure 6. Activity of miR-194 in Prostate Cancer Cells Is Mediated by Multiple Target Genes

(A) Western blot showing FOXA1 expression in LNCaP-FOXA1 or LNCaP-NC cells transfected with a miR-194 mimic or a negative control (NC).

(B) Expression of non-targetable FOXA1 partially reverses increased neurite length mediated by miR-194. Error bars are SEM; p values were determined using ANOVA (*$p < 0.05$; **$p < 0.01$; ***$p < 0.001$; ****$p < 0.0001$).

(C) Effect of non-targetable FOXA1 on miR-194-mediated changes in gene expression. Expression for NC + empty was set to 1, and error bars are SEM. p values were determined using unpaired two-sided t tests (*$p < 0.05$; **$p < 0.01$; ***$p < 0.001$). Neurite lengths, FOXA1 protein, and gene expression were measured at 96 h post-transfection.

(D) A network view of miR-194 target genes relevant to NEPC. Direct miR-194 targets are shown in blue, whereas drivers and markers of NEPC are in orange. Grey rectangles denote factors that are not miR-194 targets or documented regulators of NEPC. References documenting links between factors of interest (i.e., edges) are as follows: (1) Zhang et al. (2018), (2) Kim et al. (2017), (3) Jin et al. (2013), (4) Xu et al. (2017), (5) Lu et al. (2017), (6) Li et al. (2017b), (7) Kang et al. (2017), (8) Li et al. (2015), (9) Mertens-Talcott et al. (2007), (10) Luo et al. (2019), (11) Wu et al. (2019), (12) Dardenne et al. (2016), (13) Liang et al. (2018), (14) Satterfield et al. (2017), and (15) Li et al. (2014).

Data shown in (B) and (C) are representative of at least two independent experiments of three replicates each; error bars represent SEM. See also Figure S6.

(Das et al., 2017) and transdifferentiation from an adenocarcinoma-like cell to an NE-like cell (this study). Although this hypothesis remains to be proven, it is notable that EMT and the emergence of NE features are manifestations of cell plasticity that share many fundamental characteristics; indeed, it appears as if the re-activation of a developmental EMT program is a crucial strategy by which PCa cells evolve toward a NE lineage (Davies et al., 2018; Dicken et al., 2019). Cell plasticity leading

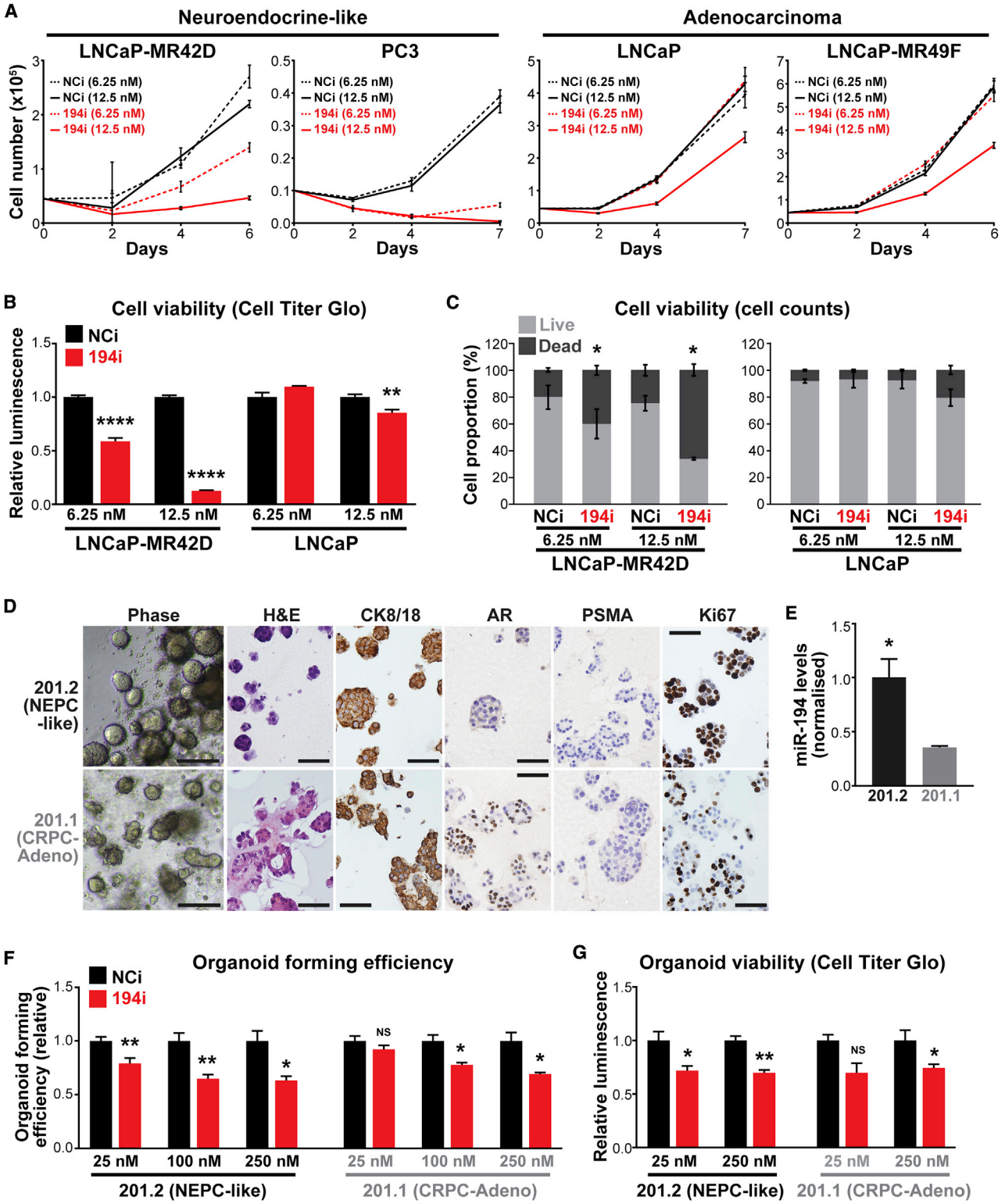

Figure 7. Inhibiting miR-194 Blocks the Growth of NEPC

(A and B) Blocking miR-194 activity with an LNA inhibitor (194i) suppresses the growth (A) and viability (B) of cell lines with neuroendocrine features (LNCaP-MR42D and PC3) more potently than AR-driven adenocarcinoma cell lines (LNCaP-MR49F and LNCaP), as determined by trypan blue growth assays and Cell

(legend continued on next page)

to NEPC could feasibly occur either by direct transdifferention or reversion to a stem-like state, followed by re-differentiation (Davies et al., 2020). Based on the relatively rapid acquisition of NE features mediated by miR-194, we propose that it is mediating direct transdifferentiation. However, it is important to note that the route to transdifferentiation is likely to be highly context dependent (Davies et al., 2020), and we have not rigorously investigated whether miR-194 can drive de-differentiation and stem-ness.

In addition to a miR-194 targetome enriched for cell movement, structure, and attachment, we identified *FOXA1* as a target gene by which miR-194 influences the emergence of NEPC. Supporting our findings, *FOXA1* is a known target of miR-194 in non-small-cell lung cancer (NSCLC); interestingly, in this context, miR-194 appears to act as a tumor suppressor, with its upregulation suppressing tumor proliferation, invasion, and metastasis (Zhu et al., 2016). The divergent outcomes of targeting FOXA1 by miR-194 in PCa and NSCLC reflects a common phenomenon in miRNA biology whereby context-dependent roles are mediated by the relative expression of key miRNA target genes in a particular cell or tissue environment. We explored the downstream consequences of FOXA1 targeting by miR-194 by using ChIP-seq, which revealed widespread alterations to the FOXA1 cistrome that were linked to de-repression of key plasticity genes, such as *SNAI2* (which encodes the Slug transcription factor), *ZEB1*, and *IL8*. Although these factors have all been implicated in NEPC (Kim et al., 2017; Jin et al., 2013; Li et al., 2014), our work reveals an additional mechanism by which they are upregulated in this disease context. A major function of FOXA1 is to serve as a pioneer factor for AR and a major regulator of its transcriptional outputs (Labbé and Brown, 2018). Like FOXA1, AR is also vital for maintenance of the epithelial phenotype; therefore, the consequent disruption of AR signaling by downregulation of FOXA1 could be another mechanism by which miR-194 enhances lineage plasticity in PCa. Combined with our finding that miR-194 is repressed by AR signaling and the identification of up to 11 AR downstream genes as miR-194 targets (Figure 2C), our study reveals a complex and intimate interplay between miR-194 and this key pathway that likely explains their strong negative correlation in clinical PCa.

Although we validated FOXA1 as a relevant target of miR-194 in terms of adenocarcinoma-NE transdifferentiation, our rescue experiments revealed that it is insufficient to explain all of the miR-194-associated phenotypes. Considering the known function of miRNAs, this result was not unexpected: not only do miRNAs have tens to hundreds of target genes but these genes are often components of the same pathway/network (Bracken et al., 2014; Liu et al., 2017; Kobayashi et al., 2019; Loeb et al., 2012), the collective targeting of which results in miRNA-mediated activity. Supporting this concept, genes with known roles in repressing the NE phenotype in PCa were enriched in the miR-194 targetome (Figure 6D). Examples include TRIM36 and ARHGAP1, which (like FOXA1) are known to regulate the ERK pathway and IL-8, respectively (Liang et al., 2018; Satterfield et al., 2017). Thus, our study highlights the propensity of an individual miRNA to target multiple nodes within the same network as a means to amplify biological outputs.

Given the increasing frequency of treatment-emergent NEPC tumors and their aggressiveness, the development of therapies that selectively target this CRPC subtype is critically important. Indeed, strategies to target AURKA (which promotes the activity of MYCN, a known driver of NEPC), EZH2 (which enhances adenocarcinoma-NEPC transdifferentiation), and the Wnt and NOTCH pathways (both of which promote stem cell maintenance in NE-like tumors) are being evaluated in clinical trials (Davies et al., 2018). Our study identifies miR-194 as a potential therapeutic target in this disease setting. Although a recent study found that miR-652 can promote the acquisition of NE features in PCa cells (Nam et al., 2018), to our knowledge, ours is the only study to date demonstrating that targeting a miRNA can inhibit NE transdifferentiation and block the growth of NEPC. Moreover, we demonstrated that overexpression of miR-194 can enhance resistance to enzalutamide and enable growth under androgen-deprived conditions, which provides a link between its pro-plasticity functions and the response of PCa cells to standard-of-care therapies. Although miRNA-based therapies have proven difficult to translate to the clinic (Fernandes et al., 2019), at least 2 antagomiRs are currently being evaluated in trials: a miR-122 antagomiR ("miravirsen") showed activity in a phase IIa trial of hepatitis C (in which no adverse side effects were reported) and a miR-155 antagomiR is in phase I trials for lymphoma (Kreth et al., 2018). The attraction of targeting miRNAs in cancer comes from the potential to concurrently modulate multiple pathways involved in tumor growth and progression. In the case of miR-194, an inhibitor could stabilize the expression of multiple plasticity-suppressing factors (e.g., FOXA1, TRIM36, and ARHGAP1) and tumor suppressors (e.g., SOCS2; Das et al., 2017), leading to inhibition of distinct plasticity- and metastasis-promoting pathways and genes (e.g., ERK, Slug, ZEB1, IL-8, and STAT3). We aim to undertake further pre-clinical evaluation of a miR-194-targeted therapy to treat NEPC and/or re-sensitize NEPC tumors to AR-targeted therapies.

Titer Glo assays, respectively. Cell Titer Glo viability assays were performed 6 days post-transfection. p values were determined using unpaired two-sided t tests (**$p < 0.01$; ****$p < 0.0001$).

(C) Proportion of live and dead cells in LNCaP-MR42D and LNCaP cells transfected with 194i or NCi for 6 days. p values were determined using unpaired two-sided t tests (*$p < 0.05$).

(D) Representative phase contrast, hematoxylin and eosin (H&E), and immunohistochemistry (IHC) of 201.1 and 201.2 organoid models growing as colonies in Matrigel. Scale bars, 100 μm (phase images) and 50 μm (H&E and IHC images).

(E) Levels of miR-194 in 201.1 and 201.2 organoids. Expression of miR-194 was normalized to two reference small RNAs (U6 and RNU44). p value was determined using an unpaired two-sided t test (*$p < 0.05$).

(F and G) Blocking miR-194 activity with 194i inhibits organoid forming efficiency (F) and organoid viability (G) of the 201.1 and 201.2 models. p values were determined using unpaired two-sided t tests. (*$p < 0.05$; **$p < 0.01$). Organoid forming efficiency and viability were assessed at day 7 post-transfection.

Data shown in (A)–(C) and (F)–(G) are representative of at least two independent experiments of three replicates each; error bars represent SEM.

In addition to its potential as a therapeutic target, it is worth noting that miR-194 was first linked to PCa as a serum marker of poor prognosis in a patients with localized disease (Selth et al., 2013). In this earlier disease context, high levels of serum miR-194 likely demarcate tumors with increased plasticity and, hence, a propensity to metastasize. However, whether miR-194 is a marker of advanced PCa and CPRC is unknown. Given the strong inverse correlation between miR-194 and AR activity, it is tempting to speculate that circulating miR-194 could be used to identify CRPC patients with AR-independent tumors (e.g., NEPC) and therefore guide therapy, but this concept remains to be tested in patient cohorts.

In summary, our study demonstrates that miR-194 can promote adenocarcinoma-NE transdifferentiation and the growth of NEPC by targeting a network of genes that includes the lineage-defining transcription factor FoxA1. These findings deliver unique molecular insights into lineage plasticity in PCa and provide impetus to investigate the potential of targeting miR-194 as a therapy for NEPC.

STAR★METHODS

Detailed methods are provided in the online version of this paper and include the following:

- KEY RESOURCES TABLE
- RESOURCE AVAILABILITY
  - Lead Contact
  - Materials Availability
  - Data and Code Availability
- EXPERIMENTAL MODEL AND SUBJECT DETAILS
  - Cell lines and cell culture
  - Organoid culture
- METHOD DETAILS
  - Cell line transfections
  - Argonaute high-throughput sequencing of RNA isolated by crosslinking immunoprecipitation (Ago-HITS-CLIP)
  - RNA sequencing
  - Gene set enrichment analysis
  - Single sample GSEA (ssGSEA)
  - Lentiviral transduction of cells
  - FOXA1 rescue experiments
  - RNA extractions
  - Quantitative RT-PCR (qRT-PCR) analysis of mRNA
  - qRT-PCR analysis of miR-194
  - Proliferation and cell viability assays
  - Neurite length measurement
  - Western blots
  - Chromatin immunoprecipitation (ChIP)-sequencing
  - Organoid transfections
- QUANTIFICATION AND STATISTICAL ANALYSIS

SUPPLEMENTAL INFORMATION

Supplemental Information can be found online at https://doi.org/10.1016/j.celrep.2020.108585.

ACKNOWLEDGMENTS

This work was supported by the National Health and Medical Research Council of Australia (1121057 to W.D.T., L.A.S., R.A.T., and G.P.R.; 1083961 to L.A.S., W.D.T., G.J.G., and P.A.G.; 1138242 to G.P.R., W.D.T., L.A.S., and M.G.L.; 1002648 to G.P.R.; 1118170 to G.J.G.) and Cancer Council South Australia (1185012 to L.A.S.). L.A.S., L.M.B., and P.A.G. are supported by Principal Cancer Research Fellowships awarded by Cancer Council's Beat Cancer project on behalf of its donors, the state Government through the Department of Health, and the Australian Government through the Medical Research Future Fund. T.E.H. is supported by an NBCF Fellowship (IIRS-19-009). M.G.L. and R.A.T. are supported by Fellowships from the Victorian Government through the Victorian Cancer Agency (MCRF18017 and MCRF15023). The research programs of L.M.B., L.A.S., and W.D.T. are supported by the Movember Foundation and the Prostate Cancer Foundation of Australia through Movember Revolutionary Team Awards.

The authors thank the Australian Cancer Research Foundation (ACRF) Cancer Genomics Facility for assistance with Ago-HITS-CLIP and RNA-seq and the South Australian Health and Medical Research Institute (SAHMRI) Genomics Facility for assistance with ChIP-seq; Geraldine Laven-Law (University of Adelaide) for expert technical assistance; Nicholas Choo (Monash University), Birunthi Niranjan (Monash University), Roxanne Toivanen (Monash University), and Susan Woods (University of Adelaide) for expert technical assistance with organoid culture; Jindan Yu (Northwestern University) for providing a FOXA1 activity gene set; Peter Nelson and Ilsa Coleman (Fred Hutchinson Cancer Research Center) for providing transcriptomic data (Bluemn et al., 2017); and Emily Hackett-Jones (University of South Australia) for assistance with analysis of the Ago-HITS-CLIP data. We acknowledge the team that generated transcriptomic data from CRPC-Adeno and NEPC tumors (Beltran et al., 2016), which we obtained from dbGaP (accession number phs000909). The results published here are in part based on data generated by The Cancer Genome Atlas, established by the National Cancer Institute and the National Human Genome Research Institute, and we are grateful to the specimen donors and relevant research groups associated with this project. Finally, we thank the patients and clinicians who have generously supported the MURAL research platform.

AUTHOR CONTRIBUTIONS

R.C.F., G.J.G., and L.A.S. conceived the project. R.C.F., P.A.G., W.D.T., T.E.H., G.J.G., and L.A.S. designed experiments. R.C.F., S.T., A.R.H., B.K.D., A.G.B., and D.O. performed experiments and acquired data. J.T. and K.A.P. performed bioinformatics analysis. R.I. and J.M.W. provided technical assistance. R.D. generated preliminary data. S.S. recruited patients for generation of PDXs. MURAL investigators established and maintained PDXs. G.P.R., R.A.T., and M.G.L. provided PDX, organoid, and serum samples. R.C.F. and L.A.S. interpreted and analyzed all data; L.M.B., A.Z., P.A.G., W.D.T., T.E.H., and G.J.G. contributed to interpreting the data. L.A.S. and R.C.F. wrote the manuscript. All of the authors have read, edited, and approved the paper.

DECLARATION OF INTERESTS

The authors declare no competing interests.

Received: October 3, 2019
Revised: October 23, 2020
Accepted: December 9, 2020
Published: January 5, 2021

REFERENCES

Abida, W., Cyrta, J., Heller, G., Prandi, D., Armenia, J., Coleman, I., Cieslik, M., Benelli, M., Robinson, D., Van Allen, E.M., et al. (2019). Genomic correlates of clinical outcome in advanced prostate cancer. Proc. Natl. Acad. Sci. USA *116*, 11428–11436.

Aggarwal, R., Huang, J., Alumkal, J.J., Zhang, L., Feng, F.Y., Thomas, G.V., Weinstein, A.S., Friedl, V., Zhang, C., Witte, O.N., et al. (2018). Clinical and Genomic Characterization of Treatment-Emergent Small-Cell Neuroendocrine Prostate Cancer: A Multi-institutional Prospective Study. J. Clin. Oncol. *36*, 2492–2503.

Aparicio, A., Logothetis, C.J., and Maity, S.N. (2011). Understanding the lethal variant of prostate cancer: power of examining extremes. Cancer Discov. *1*, 466–468.

Armenia, J., Wankowicz, S.A.M., Liu, D., Gao, J., Kundra, R., Reznik, E., Chatila, W.K., Chakravarty, D., Han, G.C., Coleman, I., et al. (2018). The long tail of oncogenic drivers in prostate cancer. Nat. Genet. *50*, 645–651.

Barbie, D.A., Tamayo, P., Boehm, J.S., Kim, S.Y., Moody, S.E., Dunn, I.F., Schinzel, A.C., Sandy, P., Meylan, E., Scholl, C., et al. (2009). Systematic RNA interference reveals that oncogenic KRAS-driven cancers require TBK1. Nature *462*, 108–112.

Beltran, H., Rickman, D.S., Park, K., Chae, S.S., Sboner, A., MacDonald, T.Y., Wang, Y., Sheikh, K.L., Terry, S., Tagawa, S.T., et al. (2011). Molecular characterization of neuroendocrine prostate cancer and identification of new drug targets. Cancer Discov. *1*, 487–495.

Beltran, H., Prandi, D., Mosquera, J.M., Benelli, M., Puca, L., Cyrta, J., Marotz, C., Giannopoulou, E., Chakravarthi, B.V., Varambally, S., et al. (2016). Divergent clonal evolution of castration-resistant neuroendocrine prostate cancer. Nat. Med. *22*, 298–305.

Bernardo, G.M., and Keri, R.A. (2012). FOXA1: a transcription factor with parallel functions in development and cancer. Biosci. Rep. *32*, 113–130.

Beshiri, M.L., Tice, C.M., Tran, C., Nguyen, H.M., Sowalsky, A.G., Agarwal, S., Jansson, K.H., Yang, Q., McGowen, K.M., Yin, J., et al. (2018). A PDX/organoid biobank of advanced prostate cancers captures genomic and phenotypic heterogeneity for disease modeling and therapeutic screening. Clin. Cancer Res. *24*, 4332–4345.

Bishop, J.L., Thaper, D., Vahid, S., Davies, A., Ketola, K., Kuruma, H., Jama, R., Nip, K.M., Angeles, A., Johnson, F., et al. (2017). The Master Neural Transcription Factor BRN2 Is an Androgen Receptor-Suppressed Driver of Neuroendocrine Differentiation in Prostate Cancer. Cancer Discov. *7*, 54–71.

Bluemn, E.G., Coleman, I.M., Lucas, J.M., Coleman, R.T., Hernandez-Lopez, S., Tharakan, R., Bianchi-Frias, D., Dumpit, R.F., Kaipainen, A., Corella, A.N., et al. (2017). Androgen Receptor Pathway-Independent Prostate Cancer Is Sustained through FGF Signaling. Cancer Cell *32*, 474–489.e6.

Bracken, C.P., Li, X., Wright, J.A., Lawrence, D.M., Pillman, K.A., Salmanidis, M., Anderson, M.A., Dredge, B.K., Gregory, P.A., Tsykin, A., et al. (2014). Genome-wide identification of miR-200 targets reveals a regulatory network controlling cell invasion. EMBO J. *33*, 2040–2056.

Broutier, L., Andersson-Rolf, A., Hindley, C.J., Boj, S.F., Clevers, H., Koo, B.-K., and Huch, M. (2016). Culture and establishment of self-renewing human and mouse adult liver and pancreas 3D organoids and their genetic manipulation. Nat. Protoc. *11*, 1724–1743.

Cancer Genome Atlas Research Network (2015). The Molecular Taxonomy of Primary Prostate Cancer. Cell *163*, 1011–1025.

Chan, S.C., Selth, L.A., Li, Y., Nyquist, M.D., Miao, L., Bradner, J.E., Raj, G.V., Tilley, W.D., and Dehm, S.M. (2015). Targeting chromatin binding regulation of constitutively active AR variants to overcome prostate cancer resistance to endocrine-based therapies. Nucleic Acids Res. *43*, 5880–5897.

Chi, S.W., Zang, J.B., Mele, A., and Darnell, R.B. (2009). Argonaute HITS-CLIP decodes microRNA-mRNA interaction maps. Nature *460*, 479–486.

Ci, X., Hao, J., Dong, X., Choi, S.Y., Xue, H., Wu, R., Qu, S., Gout, P.W., Zhang, F., Haegert, A.M., et al. (2018). Heterochromatin Protein 1α Mediates Development and Aggressiveness of Neuroendocrine Prostate Cancer. Cancer Res. *78*, 2691–2704.

Dardenne, E., Beltran, H., Benelli, M., Gayvert, K., Berger, A., Puca, L., Cyrta, J., Sboner, A., Noorzad, Z., MacDonald, T., et al. (2016). N-Myc Induces an EZH2-Mediated Transcriptional Program Driving Neuroendocrine Prostate Cancer. Cancer Cell *30*, 563–577.

Das, R., Gregory, P.A., Fernandes, R.C., Denis, I., Wang, Q., Townley, S.L., Zhao, S.G., Hanson, A.R., Pickering, M.A., Armstrong, H.K., et al. (2017). MicroRNA-194 Promotes Prostate Cancer Metastasis by Inhibiting SOCS2. Cancer Res. *77*, 1021–1034.

Davies, A.H., Beltran, H., and Zoubeidi, A. (2018). Cellular plasticity and the neuroendocrine phenotype in prostate cancer. Nat. Rev. Urol. *15*, 271–286.

Davies, A., Zoubeidi, A., and Selth, L.A. (2020). The epigenetic and transcriptional landscape of neuroendocrine prostate cancer. Endocr. Relat. Cancer *27*, R35–R50.

Delpuech, O., Rooney, C., Mooney, L., Baker, D., Shaw, R., Dymond, M., Wang, D., Zhang, P., Cross, S., Veldman-Jones, M., et al. (2016). Identification of Pharmacodynamic Transcript Biomarkers in Response to FGFR Inhibition by AZD4547. Mol. Cancer Ther. *15*, 2802–2813.

Dicken, H., Hensley, P.J., and Kyprianou, N. (2019). Prostate tumor neuroendocrine differentiation via EMT: The road less traveled. Asian J. Urol. *6*, 82–90.

Dobin, A., Davis, C.A., Schlesinger, F., Drenkow, J., Zaleski, C., Jha, S., Batut, P., Chaisson, M., and Gingeras, T.R. (2013). STAR: ultrafast universal RNA-seq aligner. Bioinformatics *29*, 15–21.

Drápela, S., Bouchal, J., Jolly, M.K., Culig, Z., and Souček, K. (2020). ZEB1: A Critical Regulator of Cell Plasticity, DNA Damage Response, and Therapy Resistance. Front. Mol. Biosci. *7*, 36.

Eichhorn, S.W., Guo, H., McGeary, S.E., Rodriguez-Mias, R.A., Shin, C., Baek, D., Hsu, S.H., Ghoshal, K., Villén, J., and Bartel, D.P. (2014). mRNA destabilization is the dominant effect of mammalian microRNAs by the time substantial repression ensues. Mol. Cell *56*, 104–115.

Fernandes, R.C., Hickey, T.E., Tilley, W.D., and Selth, L.A. (2019). Interplay between the androgen receptor signaling axis and microRNAs in prostate cancer. Endocr. Relat. Cancer *26*, R237–R257.

Gaidatzis, D., Burger, L., Florescu, M., and Stadler, M.B. (2015). Analysis of intronic and exonic reads in RNA-seq data characterizes transcriptional and post-transcriptional regulation. Nat. Biotechnol. *33*, 722–729.

Grasso, C.S., Wu, Y.M., Robinson, D.R., Cao, X., Dhanasekaran, S.M., Khan, A.P., Quist, M.J., Jing, X., Lonigro, R.J., Brenner, J.C., et al. (2012). The mutational landscape of lethal castration-resistant prostate cancer. Nature *487*, 239–243.

Guo, H., Ingolia, N.T., Weissman, J.S., and Bartel, D.P. (2010). Mammalian microRNAs predominantly act to decrease target mRNA levels. Nature *466*, 835–840.

Guo, H., Ci, X., Ahmed, M., Hua, J.T., Soares, F., Lin, D., Puca, L., Vosoughi, A., Xue, H., Li, E., et al. (2019). ONECUT2 is a driver of neuroendocrine prostate cancer. Nat. Commun. *10*, 278.

He, B., Lanz, R.B., Fiskus, W., Geng, C., Yi, P., Hartig, S.M., Rajapakshe, K., Shou, J., Wei, L., Shah, S.S., et al. (2014). GATA2 facilitates steroid receptor coactivator recruitment to the androgen receptor complex. Proc. Natl. Acad. Sci. USA *111*, 18261–18266.

Heinz, S., Benner, C., Spann, N., Bertolino, E., Lin, Y.C., Laslo, P., Cheng, J.X., Murre, C., Singh, H., and Glass, C.K. (2010). Simple combinations of lineage-determining transcription factors prime cis-regulatory elements required for macrophage and B cell identities. Mol. Cell *38*, 576–589.

Hurtado, A., Holmes, K.A., Ross-Innes, C.S., Schmidt, D., and Carroll, J.S. (2011). FOXA1 is a key determinant of estrogen receptor function and endocrine response. Nat. Genet. *43*, 27–33.

Ikeda, K., Satoh, M., Pauley, K.M., Fritzler, M.J., Reeves, W.H., and Chan, E.K. (2006). Detection of the argonaute protein Ago2 and microRNAs in the RNA induced silencing complex (RISC) using a monoclonal antibody. J. Immunol. Methods *317*, 38–44.

Jensen, K.B., and Darnell, R.B. (2008). CLIP: crosslinking and immunoprecipitation of in vivo RNA targets of RNA-binding proteins. In RNA-Protein Interaction Protocols (Springer).

Jiang, Y., Zhao, X., Xiao, Q., Liu, Q., Ding, K., Yu, F., Zhang, R., Zhu, T., and Ge, G. (2014). Snail and Slug mediate tamoxifen resistance in breast cancer cells through activation of EGFR-ERK independent of epithelial-mesenchymal transition. J. Mol. Cell Biol. *6*, 352–354.

Jin, H.J., Zhao, J.C., Ogden, I., Bergan, R.C., and Yu, J. (2013). Androgen receptor-independent function of FoxA1 in prostate cancer metastasis. Cancer Res. *73*, 3725–3736.

Kang, A.R., An, H.T., Ko, J., and Kang, S. (2017). Ataxin-1 regulates epithelial-mesenchymal transition of cervical cancer cells. Oncotarget *8*, 18248–18259.

Kim, J., Adam, R.M., and Freeman, M.R. (2002). Activation of the Erk mitogen-activated protein kinase pathway stimulates neuroendocrine differentiation in LNCaP cells independently of cell cycle withdrawal and STAT3 phosphorylation. Cancer Res. *62*, 1549–1554.

Kim, D., Pertea, G., Trapnell, C., Pimentel, H., Kelley, R., and Salzberg, S.L. (2013). TopHat2: accurate alignment of transcriptomes in the presence of insertions, deletions and gene fusions. Genome Biol. *14*, R36.

Kim, J., Jin, H., Zhao, J.C., Yang, Y.A., Li, Y., Yang, X., Dong, X., and Yu, J. (2017). FOXA1 inhibits prostate cancer neuroendocrine differentiation. Oncogene *36*, 4072–4080.

Kobayashi, M., Benakis, C., Anderson, C., Moore, M.J., Poon, C., Uekawa, K., Dyke, J.P., Fak, J.J., Mele, A., Park, C.Y., et al. (2019). AGO CLIP Reveals an Activated Network for Acute Regulation of Brain Glutamate Homeostasis in Ischemic Stroke. Cell Rep. *28*, 979–991.e6.

Kreth, S., Hübner, M., and Hinske, L.C. (2018). MicroRNAs as Clinical Biomarkers and Therapeutic Tools in Perioperative Medicine. Anesth. Analg. *126*, 670–681.

Ku, S.Y., Rosario, S., Wang, Y., Mu, P., Seshadri, M., Goodrich, Z.W., Goodrich, M.M., Labbé, D.P., Gomez, E.C., Wang, J., et al. (2017). Rb1 and Trp53 cooperate to suppress prostate cancer lineage plasticity, metastasis, and antiandrogen resistance. Science *355*, 78–83.

Kumar, A., Coleman, I., Morrissey, C., Zhang, X., True, L.D., Gulati, R., Etzioni, R., Bolouri, H., Montgomery, B., White, T., et al. (2016). Substantial interindividual and limited intraindividual genomic diversity among tumors from men with metastatic prostate cancer. Nat. Med. *22*, 369–378.

Labbé, D.P., and Brown, M. (2018). Transcriptional Regulation in Prostate Cancer. Cold Spring Harb. Perspect. Med. *8*, a030437.

Lawrence, M.G., Obinata, D., Sandhu, S., Selth, L.A., Wong, S.Q., Porter, L.H., Lister, N., Pook, D., Pezaro, C.J., Goode, D.L., et al. (2018). Patient-derived Models of Abiraterone- and Enzalutamide-resistant Prostate Cancer Reveal Sensitivity to Ribosome-directed Therapy. Eur. Urol. *74*, 562–572.

Lewis, B.P., Burge, C.B., and Bartel, D.P. (2005). Conserved seed pairing, often flanked by adenosines, indicates that thousands of human genes are microRNA targets. Cell *120*, 15–20.

Li, H., Handsaker, B., Wysoker, A., Fennell, T., Ruan, J., Homer, N., Marth, G., Abecasis, G., and Durbin, R.; 1000 Genome Project Data Processing Subgroup (2009). The sequence alignment/map format and SAMtools. Bioinformatics *25*, 2078–2079.

Li, P., Wang, J., Chu, M., Zhang, K., Yang, R., and Gao, W.Q. (2014). Zeb1 promotes androgen independence of prostate cancer via induction of stem cell-like properties. Exp. Biol. Med. (Maywood) *239*, 813–822.

Li, Y., Shen, X., Wang, X., Li, A., Wang, P., Jiang, P., Zhou, J., and Feng, Q. (2015). EGCG regulates the cross-talk between JWA and topoisomerase IIα in non-small-cell lung cancer (NSCLC) cells. Sci. Rep. *5*, 11009.

Li, J., Dantas Machado, A.C., Guo, M., Sagendorf, J.M., Zhou, Z., Jiang, L., Chen, X., Wu, D., Qu, L., Chen, Z., et al. (2017a). Structure of the Forkhead Domain of FOXA2 Bound to a Complete DNA Consensus Site. Biochemistry *56*, 3745–3753.

Li, J.P., Liu, Y., and Yin, Y.H. (2017b). ARHGAP1 overexpression inhibits proliferation, migration and invasion of C-33A and SiHa cell lines. OncoTargets Ther. *10*, 691–701.

Li, Y., Donmez, N., Sahinalp, C., Xie, N., Wang, Y., Xue, H., Mo, F., Beltran, H., Gleave, M., Wang, Y., et al. (2017c). SRRM4 Drives Neuroendocrine Transdifferentiation of Prostate Adenocarcinoma Under Androgen Receptor Pathway Inhibition. Eur. Urol. *71*, 68–78.

Liang, C., Wang, S., Qin, C., Bao, M., Cheng, G., Liu, B., Shao, P., Lv, Q., Song, N., Hua, L., et al. (2018). TRIM36, a novel androgen-responsive gene, enhances anti-androgen efficacy against prostate cancer by inhibiting MAPK/ERK signaling pathways. Cell Death Dis. *9*, 155.

Liberzon, A., Birger, C., Thorvaldsdóttir, H., Ghandi, M., Mesirov, J.P., and Tamayo, P. (2015). The Molecular Signatures Database (MSigDB) hallmark gene set collection. Cell Syst. *1*, 417–425.

Liu, C., Liu, R., Zhang, D., Deng, Q., Liu, B., Chao, H.P., Rycaj, K., Takata, Y., Lin, K., Lu, Y., et al. (2017). MicroRNA-141 suppresses prostate cancer stem cells and metastasis by targeting a cohort of pro-metastasis genes. Nat. Commun. *8*, 14270.

Loeb, G.B., Khan, A.A., Canner, D., Hiatt, J.B., Shendure, J., Darnell, R.B., Leslie, C.S., and Rudensky, A.Y. (2012). Transcriptome-wide miR-155 binding map reveals widespread noncanonical microRNA targeting. Mol. Cell *48*, 760–770.

Longair, M.H., Baker, D.A., and Armstrong, J.D. (2011). Simple Neurite Tracer: open source software for reconstruction, visualization and analysis of neuronal processes. Bioinformatics *27*, 2453–2454.

Lu, W., Liu, S., Li, B., Xie, Y., Izban, M.G., Ballard, B.R., Sathyanarayana, S.A., Adunyah, S.E., Matusik, R.J., and Chen, Z. (2017). SKP2 loss destabilizes EZH2 by promoting TRAF6-mediated ubiquitination to suppress prostate cancer. Oncogene *36*, 1364–1373.

Lun, A.T., Chen, Y., and Smyth, G.K. (2016). It's DE-licious: a recipe for differential expression analyses of RNA-seq experiments using quasi-likelihood methods in edgeR. Statistical Genomics (Springer).

Luo, J., Wang, K., Yeh, S., Sun, Y., Liang, L., Xiao, Y., Xu, W., Niu, Y., Cheng, L., Maity, S.N., et al. (2019). LncRNA-p21 alters the antiandrogen enzalutamide-induced prostate cancer neuroendocrine differentiation via modulating the EZH2/STAT3 signaling. Nat. Commun. *10*, 2571.

Martin, M. (2011). Cutadapt removes adapter sequences from high-throughput sequencing reads. EMBnet. J. *17*, 10–12.

Meerbrey, K.L., Hu, G., Kessler, J.D., Roarty, K., Li, M.Z., Fang, J.E., Herschkowitz, J.I., Burrows, A.E., Ciccia, A., Sun, T., et al. (2011). The pINDUCER lentiviral toolkit for inducible RNA interference in vitro and in vivo. Proc. Natl. Acad. Sci. USA *108*, 3665–3670.

Meijering, E., Jacob, M., Sarria, J.C., Steiner, P., Hirling, H., and Unser, M. (2004). Design and validation of a tool for neurite tracing and analysis in fluorescence microscopy images. Cytometry A *58*, 167–176.

Mertens-Talcott, S.U., Chintharlapalli, S., Li, X., and Safe, S. (2007). The oncogenic microRNA-27a targets genes that regulate specificity protein transcription factors and the G2-M checkpoint in MDA-MB-231 breast cancer cells. Cancer Res. *67*, 11001–11011.

Moore, N.L., Buchanan, G., Harris, J.M., Selth, L.A., Bianco-Miotto, T., Hanson, A.R., Birrell, S.N., Butler, L.M., Hickey, T.E., and Tilley, W.D. (2012). An androgen receptor mutation in the MDA-MB-453 cell line model of molecular apocrine breast cancer compromises receptor activity. Endocr. Relat. Cancer *19*, 599–613.

Mu, P., Zhang, Z., Benelli, M., Karthaus, W.R., Hoover, E., Chen, C.C., Wongvipat, J., Ku, S.Y., Gao, D., Cao, Z., et al. (2017). SOX2 promotes lineage plasticity and antiandrogen resistance in TP53- and RB1-deficient prostate cancer. Science *355*, 84–88.

Nam, R.K., Benatar, T., Amemiya, Y., Wallis, C.J.D., Romero, J.M., Tsagaris, M., Sherman, C., Sugar, L., and Seth, A. (2018). MicroRNA-652 induces NED in LNCaP and EMT in PC3 prostate cancer cells. Oncotarget *9*, 19159–19176.

Osada, H., Tomida, S., Yatabe, Y., Tatematsu, Y., Takeuchi, T., Murakami, H., Kondo, Y., Sekido, Y., and Takahashi, T. (2008). Roles of achaete-scute homologue 1 in DKK1 and E-cadherin repression and neuroendocrine differentiation in lung cancer. Cancer Res. *68*, 1647–1655.

Paltoglou, S., Das, R., Townley, S.L., Hickey, T.E., Tarulli, G.A., Coutinho, I., Fernandes, R., Hanson, A.R., Denis, I., Carroll, J.S., et al. (2017). Novel Androgen Receptor Coregulator GRHL2 Exerts Both Oncogenic and Antimetastatic Functions in Prostate Cancer. Cancer Res. *77*, 3417–3430.

Pillman, K.A., Phillips, C.A., Roslan, S., Toubia, J., Dredge, B.K., Bert, A.G., Lumb, R., Neumann, D.P., Li, X., Conn, S.J., et al. (2018). miR-200/375 control

epithelial plasticity-associated alternative splicing by repressing the RNA-binding protein Quaking. EMBO J. *37*, e99016.

Pillman, K.A., Scheer, K.G., Hackett-Jones, E., Saunders, K., Bert, A.G., Toubia, J., Whitfield, H.J., Sapkota, S., Sourdin, L., Pham, H., et al. (2019). Extensive transcriptional responses are co-ordinated by microRNAs as revealed by Exon-Intron Split Analysis (EISA). Nucleic Acids Res. *47*, 8606–8619.

Pomerantz, M.M., Li, F., Takeda, D.Y., Lenci, R., Chonkar, A., Chabot, M., Cejas, P., Vazquez, F., Cook, J., Shivdasani, R.A., et al. (2015). The androgen receptor cistrome is extensively reprogrammed in human prostate tumorigenesis. Nat. Genet. *47*, 1346–1351.

Porter, L.H., Lawrence, M.G., Wang, H., Clark, A.K., Bakshi, A., Obinata, D., Goode, D., Papargiris, M., Mural, Clouston, D., et al. (2019). Establishing a cryopreservation protocol for patient-derived xenografts of prostate cancer. Prostate *79*, 1326–1337.

Qi, J., Nakayama, K., Cardiff, R.D., Borowsky, A.D., Kaul, K., Williams, R., Krajewski, S., Mercola, D., Carpenter, P.M., Bowtell, D., and Ronai, Z.A. (2010). Siah2-dependent concerted activity of HIF and FoxA2 regulates formation of neuroendocrine phenotype and neuroendocrine prostate tumors. Cancer Cell *18*, 23–38.

Recine, F., and Sternberg, C.N. (2015). Hormonal therapy and chemotherapy in hormone-naive and castration resistant prostate cancer. Transl. Androl. Urol. *4*, 355–364.

Robinson, M.D., McCarthy, D.J., and Smyth, G.K. (2010). edgeR: a Bioconductor package for differential expression analysis of digital gene expression data. Bioinformatics *26*, 139–140.

Robinson, J.L., Hickey, T.E., Warren, A.Y., Vowler, S.L., Carroll, T., Lamb, A.D., Papoutsoglou, N., Neal, D.E., Tilley, W.D., and Carroll, J.S. (2014). Elevated levels of FOXA1 facilitate androgen receptor chromatin binding resulting in a CRPC-like phenotype. Oncogene *33*, 5666–5674.

Robinson, D., Van Allen, E.M., Wu, Y.M., Schultz, N., Lonigro, R.J., Mosquera, J.M., Montgomery, B., Taplin, M.E., Pritchard, C.C., Attard, G., et al. (2015). Integrative clinical genomics of advanced prostate cancer. Cell *161*, 1215–1228.

Ross-Innes, C.S., Stark, R., Teschendorff, A.E., Holmes, K.A., Ali, H.R., Dunning, M.J., Brown, G.D., Gojis, O., Ellis, I.O., Green, A.R., et al. (2012). Differential oestrogen receptor binding is associated with clinical outcome in breast cancer. Nature *481*, 389–393.

Satterfield, L., Shuck, R., Kurenbekova, L., Allen-Rhoades, W., Edwards, D., Huang, S., Rajapakshe, K., Coarfa, C., Donehower, L.A., and Yustein, J.T. (2017). miR-130b directly targets ARHGAP1 to drive activation of a metastatic CDC42-PAK1-AP1 positive feedback loop in Ewing sarcoma. Int. J. Cancer *141*, 2062–2075.

Schindelin, J., Arganda-Carreras, I., Frise, E., Kaynig, V., Longair, M., Pietzsch, T., Preibisch, S., Rueden, C., Saalfeld, S., Schmid, B., et al. (2012). Fiji: an open-source platform for biological-image analysis. Nat. Methods *9*, 676–682.

Selbach, M., Schwanhäusser, B., Thierfelder, N., Fang, Z., Khanin, R., and Rajewsky, N. (2008). Widespread changes in protein synthesis induced by microRNAs. Nature *455*, 58–63.

Selth, L.A., Townley, S.L., Bert, A.G., Stricker, P.D., Sutherland, P.D., Horvath, L.G., Goodall, G.J., Butler, L.M., and Tilley, W.D. (2013). Circulating microRNAs predict biochemical recurrence in prostate cancer patients. Br. J. Cancer *109*, 641–650.

Shen, R., Dorai, T., Szaboles, M., Katz, A.E., Olsson, C.A., and Buttyan, R. (1997). Transdifferentiation of cultured human prostate cancer cells to a neuroendocrine cell phenotype in a hormone-depleted medium. Urol. Oncol. *3*, 67–75.

Smith, B.N., Burton, L.J., Henderson, V., Randle, D.D., Morton, D.J., Smith, B.A., Taliaferro-Smith, L., Nagappan, P., Yates, C., Zayzafoon, M., et al. (2014). Snail promotes epithelial mesenchymal transition in breast cancer cells in part via activation of nuclear ERK2. PLoS One *9*, e104987.

Song, B., Park, S.H., Zhao, J.C., Fong, K.W., Li, S., Lee, Y., Yang, Y.A., Sridhar, S., Lu, X., Abdulkadir, S.A., et al. (2019). Targeting FOXA1-mediated repression of TGF-β signaling suppresses castration-resistant prostate cancer progression. J. Clin. Invest. *129*, 569–582.

Sowalsky, A.G., Ye, H., Bhasin, M., Van Allen, E.M., Loda, M., Lis, R.T., Montaser-Kouhsari, L., Calagua, C., Ma, F., Russo, J.W., et al. (2018). Neoadjuvant-Intensive Androgen Deprivation Therapy Selects for Prostate Tumor Foci with Diverse Subclonal Oncogenic Alterations. Cancer Res. *78*, 4716–4730.

Su, S., Law, C.W., Ah-Cann, C., Asselin-Labat, M.-L., Blewitt, M.E., and Ritchie, M.E. (2017). Glimma: interactive graphics for gene expression analysis. Bioinformatics *33*, 2050–2052.

Subramanian, A., Tamayo, P., Mootha, V.K., Mukherjee, S., Ebert, B.L., Gillette, M.A., Paulovich, A., Pomeroy, S.L., Golub, T.R., Lander, E.S., and Mesirov, J.P. (2005). Gene set enrichment analysis: a knowledge-based approach for interpreting genome-wide expression profiles. Proc. Natl. Acad. Sci. USA *102*, 15545–15550.

Taylor, B.S., Schultz, N., Hieronymus, H., Gopalan, A., Xiao, Y., Carver, B.S., Arora, V.K., Kaushik, P., Cerami, E., Reva, B., et al. (2010). Integrative genomic profiling of human prostate cancer. Cancer Cell *18*, 11–22.

Thorvaldsdóttir, H., Robinson, J.T., and Mesirov, J.P. (2013). Integrative Genomics Viewer (IGV): high-performance genomics data visualization and exploration. Brief. Bioinform. *14*, 178–192.

Tsai, H.K., Lehrer, J., Alshalalfa, M., Erho, N., Davicioni, E., and Lotan, T.L. (2017). Gene expression signatures of neuroendocrine prostate cancer and primary small cell prostatic carcinoma. BMC Cancer *17*, 759.

Van Nostrand, E.L., Pratt, G.A., Shishkin, A.A., Gelboin-Burkhart, C., Fang, M.Y., Sundararaman, B., Blue, S.M., Nguyen, T.B., Surka, C., Elkins, K., et al. (2016). Robust transcriptome-wide discovery of RNA-binding protein binding sites with enhanced CLIP (eCLIP). Nat. Methods *13*, 508–514.

Vidal, S.J., Rodriguez-Bravo, V., Quinn, S.A., Rodriguez-Barrueco, R., Lujambio, A., Williams, E., Sun, X., de la Iglesia-Vicente, J., Lee, A., Readhead, B., et al. (2015). A targetable GATA2-IGF2 axis confers aggressiveness in lethal prostate cancer. Cancer Cell *27*, 223–239.

Wang, Q., Li, W., Zhang, Y., Yuan, X., Xu, K., Yu, J., Chen, Z., Beroukhim, R., Wang, H., Lupien, M., et al. (2009). Androgen receptor regulates a distinct transcription program in androgen-independent prostate cancer. Cell *138*, 245–256.

Wu, P.Y., Yu, I.S., Lin, Y.C., Chang, Y.T., Chen, C.C., Lin, K.H., Tseng, T.H., Kargren, M., Tai, Y.L., Shen, T.L., et al. (2019). Activation of Aryl Hydrocarbon Receptor by Kynurenine Impairs Progression and Metastasis of Neuroblastoma. Cancer Res. *79*, 5550–5562.

Xu, J., Zhou, W., Yang, F., Chen, G., Li, H., Zhao, Y., Liu, P., Li, H., Tan, M., Xiong, X., and Sun, Y. (2017). The β-TrCP-FBXW2-SKP2 axis regulates lung cancer cell growth with FBXW2 acting as a tumour suppressor. Nat. Commun. *8*, 14002.

Yuan, S., Norgard, R.J., and Stanger, B.Z. (2019). Cellular Plasticity in Cancer. Cancer Discov. *9*, 837–851.

Zhang, Y., Liu, T., Meyer, C.A., Eeckhoute, J., Johnson, D.S., Bernstein, B.E., Nusbaum, C., Myers, R.M., Brown, M., Li, W., and Liu, X.S. (2008). Model-based analysis of ChIP-Seq (MACS). Genome Biol. *9*, R137.

Zhang, Y., Zheng, D., Zhou, T., Song, H., Hulsurkar, M., Su, N., Liu, Y., Wang, Z., Shao, L., Ittmann, M., et al. (2018). Androgen deprivation promotes neuroendocrine differentiation and angiogenesis through CREB-EZH2-TSP1 pathway in prostate cancers. Nat. Commun. *9*, 4080.

Zhu, X., Li, D., Yu, F., Jia, C., Xie, J., Ma, Y., Fan, S., Cai, H., Luo, Q., Lv, Z., and Fan, L. (2016). miR-194 inhibits the proliferation, invasion, migration, and enhances the chemosensitivity of non-small cell lung cancer cells by targeting forkhead box A1 protein. Oncotarget *7*, 13139–13152.

STAR★METHODS

KEY RESOURCES TABLE

REAGENT or RESOURCE	SOURCE	IDENTIFIER
Antibodies		
Rabbit polyclonal anti FOXA1	Abcam	Cat# ab23738; RRID:AB_2104842
Rabbit monoclonal anti p44/42 MAPK (Erk1/2)	Cell Signaling Technology	Cat# 4695P; RRID:AB_390779
Rabbit monoclonal anti phospho p44/42 MAPK (Erk1/2) (Thr202/Tyr204)	Cell Signaling Technology	Cat#: 4370P; RRID:AB_2315112
Mouse monoclonal anti GAPDH	Merck Millipore	Cat# MAB374; RRID:AB_2107445
HRP conjugated anti rabbit IgG	Dako	Cat# P0448; RRID:AB_2617138
HRP conjugated anti mouse IgG	Dako	Cat# P0161; RRID:AB_2687969
Biological Samples		
Patient Derived Xenografts	Lawrence et al., 2018 (Melbourne Urological Research Alliance)	N/A
Chemicals, Peptides, and Recombinant Proteins		
Anti-microRNA-194 inhibitors (LNA)	QIAGEN	Cat# YI04101208-DFA
Anti-microRNA negative control LNA inhibitors	QIAGEN	Cat# YI00199006-DFA
Lipofectamine RNA iMAX	Invitrogen	Cat# 13778150
Matrigel Growth Factor Reduced	Corning Scientific	Cat# BD 356231
mirVana® miRNA mimic hsa-miR-194-5p	Ambion	Cat# 4464066
mirVana® miRNA mimic negative control	Ambion	Cat# 4464058
Pre-microRNA-194 precursors	GenePharma	Cat# B02001
Pre-microRNA precursors negative control	GenePharma	Cat# B04002
TRI reagent	Sigma	Cat# T9424
Critical Commercial Assays		
CellTiter-Glo Luminescent Cell Viability Assay	Promega	Cat# G7572
iScript cDNA synthesis kit	Bio-Rad	Cat# 170-8891
iQ SYBR Green Supermix	Bio-Rad	Cat# 170-8885
TaqMan MicroRNA Reverse Transcription Kit	Applied Biosystems	Cat# 4366596
Hsa-miR-194 Taqman Assay ID: 000493	Thermo Fisher Scientific	Cat# 4427975
U6 snRNA Taqman Assay ID: 001973	Thermo Fisher Scientific	Cat# 4427975
RNU44 Taqman Assay ID: 001094	Thermo Fisher Scientific	Cat# 4427975
TaqMan Universal Master Mix II, no UNG	Applied Biosystems	Cat# 4440040
Turbo DNA-Free kit	Invitrogen	Cat# AM2238
Deposited Data		
Raw and analyzed data	This paper	GEO: GSE137072
Experimental Models: Cell Lines		
22RV1	ATCC	Cat# CRL-2505
LNCaP	ATCC	Cat# CRL-1740
PC3	ATCC	Cat# CRL-1435
LNCaP-MR42D	Bishop et al., 2017	N/A
LNCaP-V16D	Bishop et al., 2017	N/A
LNCaP-MR49F	Bishop et al., 2017	N/A
201.1 organoids	Lawrence et al., 2018 (Melbourne Urological Research Alliance)	N/A

(*Continued on next page*)

Continued

REAGENT or RESOURCE	SOURCE	IDENTIFIER
201.2 organoids	Lawrence et al., 2018 (Melbourne Urological Research Alliance)	N/A
Oligonucleotides		
Listed in Table S6	Sigma	N/A
Recombinant DNA		
pInducer10-miR-194	This paper	N/A
pInducer10-scrambled control	This paper	N/A
pcDNA-FOXA1	Hurtado et al., 2011 (Dr. Jason Carroll, Cancer Research UK, Cambridge Institute)	N/A
pCDNA3.1 (-) (pcDNA-Empty)	Thermo Fisher Scientific	Cat #: V79520
pCW57.1-FOXA1	This paper	N/A
pCW57.1-Empty	This paper	N/A
pCW57.1	David Root Lab; pLEX and pLIX Gateway backbones (unpublished)	RRID:Addgene_41393
Software and Algorithms		
cutadapt v1.8.1	Martin, 2011	https://cutadapt.readthedocs.io/en/stable/
DiffBind	Ross-Innes et al., 2012	https://bioconductor.org/packages/release/bioc/html/DiffBind.html
EdgeR	Robinson et al., 2010	http://bioconductor.org/packages/release/bioc/html/edgeR.html
FastQC		http://www.bioinformatics.babraham.ac.uk/projects/fastqc
Glimma	Su et al., 2017	http://bioconductor.org/packages/release/bioc/html/Glimma.html
Homer	Heinz et al., 2010	http://homer.ucsd.edu/homer/
ImageJ (Fiji)	Schindelin et al., 2012	https://imagej.net/Welcome
Integrative Genomics Viewer	Thorvaldsdóttir et al., 2013	http://software.broadinstitute.org/software/igv/
MACS2 peak caller	Zhang et al., 2008	N/A
NeuronJ	Meijering et al., 2004	https://imagescience.org/meijering/software/neuronj/
Prism	GraphPad	https://www.graphpad.com/scientific-software/prism/
Simple Neurite Tracer	Longair et al., 2011	https://imagej.net/SNT
STAR spliced alignment algorithm	Dobin et al., 2013	N/A
TopHat2	Kim et al., 2013	https://ccb.jhu.edu/software/tophat/index.shtml

RESOURCE AVAILABILITY

Lead Contact

Further information and requests for resources and reagents should be directed to and will be fulfilled by the Lead Contact, Luke A. Selth (luke.selth@flinders.edu.au).

Materials Availability

Materials generated in this study are available upon reasonable request from the lead contact.

Data and Code Availability

Ago-HITS-CLIP, RNA-seq and ChIP-seq datasets generated during this study are available from NCBI's Gene Expression Omnibus (GEO: GSE137072). This study did not generate any unique code.

EXPERIMENTAL MODEL AND SUBJECT DETAILS

Cell lines and cell culture

LNCaP, PC3 and 22RV1 cell lines were purchased from the American Type Culture Collection (ATCC). LNCaP-MR42D and LNCaP-MR49F cell lines have been described previously (Bishop et al., 2017). All cell lines used in this study were derived from males. LNCaP and 22RV1 cell lines were maintained in RPMI-1640 (Sigma) containing 10% Fetal Bovine Serum (FBS) (Sigma) at 37°C. PC3 cell lines were maintained in RPMI-1640 containing 5% FBS at 37°C. LNCaP-MR42D and LNCaP-MR49F cells were maintained in RPMI-1640 containing 10% FBS and 10 μM Enzalutamide at 37°C. For serum starvation experiments, cells were grown in phenol red-free RPMI-1640 containing 10% dextran-coated charcoal (DCC) stripped serum at 37°C. Cell lines were subjected to regular mycoplasma testing. All cell lines underwent authentication by short tandem repeat profiling by CellBank Australia.

Organoid culture

PDXs were established by the Melbourne Urology Research Alliance (MURAL) (Monash University Human Research Ethics Committee approval 12287). The established PDXs were grown as subcutaneous grafts in male NSG mice supplemented with testosterone implants according to animal ethics approval (17963), as previously described (Lawrence et al., 2018; Porter et al., 2019). PDXs were routinely authenticated using short tandem repeat profiling (GenePrint 10, Promega) at the Australian Genome Research Facility. Tissue from PDXs 201.1 dura (adenocarcinoma) and 201.2 lung (AR null) was digested and grown as organoids in growth factor reduced, phenol red-free, ldEV-free Matrigel (Corning). 201.1 organoids were cultured in advanced DMEM/F-12 media (GIBCO) containing 0.1 mg/ml Primocin (Invivogen), 1x Glutamax (GIBCO), 10 mM HEPES (GIBCO), 1 nM DHT (Sigma), 1.25mM N-acetylcysteine (Sigma), 5nM NRG1 Heregulinβ-1 (Peprotech), 500 nM A83-01 (Sigma), 10 mM nicotinamide (Sigma), 0.5 μM SB202190 (Sigma), 2% B27 (Thermo), 20 ng/ml FGF10 (Peprotech), 5 ng/ml FGF7 (Peprotech), 10ng/ml Amphiregulin (Peprotech), 1 μM prostaglandin E2 (Tocris), 10% noggin conditioned media and 10% R-spondin conditioned media. 201.2 Lung organoids were cultured in PrENR -p38i -NAC media (Beshiri et al., 2018). 10 μM Y-27632 dihydrochloride (Selleck Chemicals) was added to culture medium during organoid establishment and following passage.

METHOD DETAILS

Cell line transfections

Transient transfection of cell lines were performed using RNAiMAX Transfection Reagent (Invitrogen) according to the manufacturer's instructions. For HITS-CLIP and RNA-seq experiments, 22RV1 cells were transfected with 20nM miRVana mimic (miR-194 or negative control; Ambion). For all other experiments, cells were transfected with 20nM miRNA mimics from Shanghai GenePharma. For miR-194 inhibition, cells were transfected with 12.5 or 6.25nM locked nucleic acid (LNA) miRNA inhibitors (miR-194 LNA inhibitor or negative control inhibitor; QIAGEN).

Argonaute high-throughput sequencing of RNA isolated by crosslinking immunoprecipitation (Ago-HITS-CLIP)

The Ago-HITS-CLIP method was adapted from published methods (Chi et al., 2009; Jensen and Darnell, 2008), incorporating modifications from eCLIP (Van Nostrand et al., 2016; Pillman et al., 2018). 22RV1 cells were seeded in 10 cm cell culture dishes and transfected in suspension with 20 nM miRVana mimic (miR-194 or negative control, 3 replicates of each; Ambion) using RNAiMAX (Invitrogen). After 24 h, transfected 22RV1 cells were rinsed once with ice-cold PBS and UV irradiated with 600 mJ/cm2, 254 nm, in ice-cold PBS using a UV Stratalinker-1800 (Agilent). Cells were collected by scraping, and cell pellets stored at −80°C as one pellet per 100mm plate. One pellet per CLIP IP was lysed in 500 μL of 1 X PXL (1 X PBS, 0.1% SDS, 0.5% deoxycholate, 0.5% Igepal) + EDTA-free Complete protease inhibitor cocktail (PIC; Roche) for 15 min on ice, followed by trituration through a 21G needle and syringe 5 times. DNA was digested with 20 μL RQ1 DNase (Promega) at 37°C for 10 min on a Thermomixer (750 rpm, Eppendorf). RNA was partially digested with RNase 1 (ThermoFisher) by adding 5 μL of 1:40 diluted RNase 1 in 1 X PBS at 37°C for 5 min on a Thermomixer (750 rpm), then returned to ice. Lysates were centrifuged at 21,000 g for 20 min at 4°C and supernatant transferred to a fresh tube.

AGO-RNA complexes were immunoprecipitated using mouse IgA2 monoclonal anti-Ago2 antibody 4F9 (Ikeda et al., 2006); hybridoma sourced from University of Florida ICBR) with a mouse IgA antibody (GeneTex S107) used as a control. Antibodies (8 μg) were conjugated to 20 μL protein L Dynabeads (ThermoFisher, 88849) in PBS-Tw (1 X PBS, 0.05% Tween-20) for 45 min and washed three times with 1 X PXL (1 X PBS, 0.1% SDS, 0.5% sodium deoxycholate, 0.5% Igepal) before resuspending the beads with 450 μL of prepared lysate and rotating for 2 hr at 4°C. Bound AGO-RNA complexes were washed twice each consecutively with ice cold 1 X PXL, 5 X PXL (5 X PBS, 0.1% SDS, 0.5% sodium deoxycholate, 0.5% Igepal), and 1 X PNK (50 mM Tris-Cl pH 7.5, 10 mM MgCl2, and 0.5% Igepal). Beads were first treated with T4 PNK (NEB, M0201L; 20 U in 80 μL reaction volume) in the absence of ATP (37°C, 850 rpm for 20 min) to dephosphorylate 3′ RNA ends followed by washes with 1 X PNK, 5 X PXL, and two washes with 1 X PNK at 4°C. The 3′ preadenylated linker (NEBNext 3′SR adaptor for Illumina; /5rApp/AGA TCG GAA GAG CAC ACG TCT /3AmMO/) was ligated to the RNA fragments on bead using T4 RNA ligase 2 truncated KQ (NEB M0373; 100 U in a 40 μL reaction

volume, 12% PEG8000, 1x RNA ligase buffer, 0.125 μM adaptor) in the absence of ATP at 16°C, overnight with periodic mixing. Beads were washed consecutively with ice cold 1 X PXL, 5 X PXL, and twice with 1 X PNK. Bound RNAs were then labeled with P32 γ-ATP using T4 PNK, 20 min at 37°C, and washed as above.

AGO-RNA complexes were eluted with 40 μL 1 X Bolt LDS sample buffer (ThermoFisher) + 1% β-mercaptoethanol at 70°C for 10 min on a Thermomixer (1200 rpm). Samples were separated through Bolt 8% Bis-tris Plus gels (ThermoFisher) using BOLT MOPS SDS running buffer at 200 V for 75 min. Complexes were then transferred to nitrocellulose (Schleicher&Schuell, BA-85) by wet transfer using 1 X BOLT transfer buffer with 10% methanol. Filters were placed on a phosphor screen and exposed using a Typhoon imager (GE). 115-160 kDa regions (corresponding to RNA tags > 30 nt) were excised from the nitrocellulose. RNA was extracted by proteinase K digestion (2 mg/mL proteinase K, 100 mM Tris-HCl pH 7.5, 50 mM NaCl, 10 mM EDTA, 0.2% SDS) at 50°C for 60 min on a Thermomixer (1200 rpm) followed by extraction with acid phenol (ThermoFisher, AM9712) and precipitation with 1:1 isopropanol:ethanol. RNA was pelleted by centrifugation then separated on a 15% denaturing polyacrylamide gel (1:19 acrylamide, 1 X TBE, 7 M urea). The wet gel was wrapped in plastic wrap and exposed to a phosphor screen and imaged using a Typhoon. Gel slices were cut corresponding to the expected size of the cross-linked RNA eluted by the ''crush and soak'' method as previously described (Jensen and Darnell, 2008).

Reverse transcription, 5′ linker ligation and amplification were performed essentially as previously described (Van Nostrand et al., 2016) using SR-RT primer for reverse transcription (IDT, AGACGTGTGCTCTTCCGATCT) with SuperScript IV, and a custom synthesized 5′ linker (IDT, 5′SRdeg /5Phos/NN NNN NNN NNG ATC GTC GGA CTG TAG AAC TCT GAA C/3SpC3/). Products were amplified for 20 cycles using a common forward primer (NEBNext SR primer for Illumina) and barcoded reverse primers for each sample (NEBNext Index primers for Illumina). PCR products were purified using QIAGEN Qiaquick PCR purification kit, separated on an 8% acrylamide (29:1) TBE non- denaturing gel, stained with SYBR Gold nucleic acid gel stain (ThermoFisher) and imaged on a ChemiDoc (BioRad). Products corresponding to an insert size of ~30 – 70 nt were excised from the gel and extracted by the ''crush and soak'' method as previously described (Jensen and Darnell, 2008). Library quality and quantity was assessed by Bioanalyzer (Agilent) and qPCR, pooled and sequenced on an Illumina NextSeq 500 (1 × 75bp) at the Australian Cancer Research Foundation (ACRF) Cancer Genomics Facility.

RNA libraries generated by HITS-CLIP were sequenced on the Illumina Nextseq 500 platform using the single end protocol with a read length of 75. Raw reads were adaptor trimmed and filtered for short sequences using cutadapt v1.8.1 (Martin, 2011) setting minimum-length option to 18, error-rate 0.2, and overlap 5. The resulting FASTQ files (averaging 41.6 million reads per sample) were analyzed and quality checked using the FastQC (http://www.bioinformatics.babraham.ac.uk/projects/fastqc) program. Filtered reads were mapped against the human reference genome (hg19) using the Tophat2 alignment algorithm (version 2.0.9 with default parameters) (Kim et al., 2013), returning an average alignment rate of 43.8%. Unique molecular identifiers (UMIs) were used to deduplicate reads that mapped to the same start site, possessed identical CIGAR strings and UMI barcodes sequences $\leq$ 1 edit distance apart. Enriched regions of the genome were identified from Samtools quality-filtered alignments (Li et al., 2009) (-q 5) with the MACS2 peak caller (version 2.1.1) (Zhang et al., 2008) (setting;–nomodel,–shift −15,–extsize 50, -B,–slocal 0,–llocal 0,–fe-cutoff 10, -q 0.05). Peak calling was performed using pooled alignment files and carried out separately for each strand. The resulting peak files from each strand were merged. Features in the vicinity of peak loci and enrichment of motifs within peaks were determined and analyzed using Homer (Heinz et al., 2010). Alignments were visualized and interrogated using IGV (Thorvaldsdóttir et al., 2013).

CLIP using a control antibody was performed on a single biological replicate of control transfected cells but yielded very little sequence data and was excluded from the analysis.

RNA sequencing

22RV1 cells were seeded in 6-well plates and transfected in solution with 20nM miRVana mimic (miR-194 or negative control; Ambion) using RNAiMAX (Invitrogen). At 36 hours post-transfection, cells were collected in Qiazol (QIAGEN) and total RNA was extracted using a miRNeasy Mini Kit (QIAGEN) according to the manufacturer's instructions. RNA seq was performed on 4 biological replicates each of 22RV1 cells transfected with miR-194 or negative control. RNA sequencing libraries were constructed with the mRNaseq Library prep kit and libraries were sequenced on the Illumina NextSeq 500 platform at the Australian Cancer Research Foundation (ACRF) Cancer Genomics Facility.

RNA-seq libraries were multiplexed and sequenced on the Illumina NextSeq 500 platform using the stranded, paired-end protocol with a read length of 150. Raw reads were adaptor trimmed and filtered for short sequences using cutadapt v1.8.1 (Martin, 2011), setting minimum-length option to 18, error-rate 0.2, quality cut-off 28, overlap 5 and trim N's on. The resulting FASTQ files (averaging 60.2 million read pairs per sample) were analyzed and quality checked using the FastQC program (http://www.bioinformatics.babraham.ac.uk/projects/fastqc). Reads were mapped against the human reference genome (hg19) using the STAR spliced alignment algorithm (Dobin et al., 2013) (version 2.5.3a with default parameters and–chimSegmentMin 20,–quantMode GeneCounts), returning an average unique alignment rate of 92.9%. Differential expression analysis was evaluated from TMM normalized gene counts using R (version 3.2.3) and edgeR (Robinson et al., 2010) (version 3.3), following protocols as described (Lun et al., 2016). Graphical representations of differentially expressed genes were generated using Glimma (Su et al., 2017). Alignments were visualized and interrogated using the Integrative Genomics Viewer v2.3.80 (Thorvaldsdóttir et al., 2013).

Exon Intron Split analysis (EISA) was performed as described previously (Pillman et al., 2019). To refine the miR-194 targetome, only post-transcriptionally downregulated genes (i.e., genes with log2FC(dExon-dIntron) < 0) and a FDR cutoff of 0.05) were considered as targets.

Gene set enrichment analysis

Genes were ranked according to expression using the Signal2Noise metric. Gene Set Enrichment Analysis (Preranked analysis) (Subramanian et al., 2005) was implemented using the Broad Institute's public GenePattern server with default parameters.

Single sample GSEA (ssGSEA)

Expression data was downloaded from GEO (Kumar 2016 (GEO: GSE77930) (Kumar et al., 2016)), cBioportal (MSKCC (Taylor et al., 2010) and SU2C (Robinson et al., 2015)), TCGA (Cancer Genome Atlas Research Network, 2015) and dbGAP (Beltran et al., 2016). ssGSEA (Barbie et al., 2009) was implemented using the Broad Institute's public GenePattern server, using rank normalization and default parameters. Since miRNAs repress expression of their target genes, miR-194 activity was calculated as the inverse value of ssGSEA scores for the miR-194 targetome.

Lentiviral transduction of cells

To generate doxycycline-inducible miR-194 overexpressing LNCaP cells, the pre-miR-194 sequence or a scrambled control sequence were cloned into the pInducer10 lentiviral vector (Meerbrey et al., 2011). Lentivirus particles were prepared using a third-generation packaging system in HEK293T cells by transfection of cells with packaging vector and pInducer10 vectors. LNCaP cells were transduced with concentrated lentivirus at a MOI of 1 followed by one week of puromycin selection to generate doxycycline-inducible LNCaP-194 and LNCaP-NC cells. Cells were grown in 1 μg per ml of doxycycline to induce miR-194 expression.

To generate doxycycline-inducible FOXA1 overexpressing LNCaP cells, the FOXA1 ORF was cloned into the pCW57.1 lentiviral vector using Gateway cloning. Empty pCW57.1 vector was used to generate control cell lines. Production of lentiviral particles and viral transduction was carried out as described above.

FOXA1 rescue experiments

Rescue experiments in stable LNCaP-derived cell lines were performed by transfecting LNCaP-FOXA1 or LNCaP-Empty cells with 20 nM miR-194 or negative control (Shanghai GenePharma) in solution using RNAiMAX Transfection Reagent (Invitrogen) for 96 hours. 250 ng per ml of doxycycline was added to cell growth media at the time of transfection and again at 48 hours. Rescue experiments in the 22Rv1 model were performed by co-transfecting 22Rv1 cells with 20 nM miR-194 (or negative control) and 100 ng pcDNA-FOXA1 (Hurtado et al., 2011) (or pcDNA-Empty) in solution using RNAiMAX for 96 hours.

RNA extractions

Total RNA from cell lines was extracted using TRI Reagent (Sigma) as described previously (Das et al., 2017). PDX tissues preserved in RNALater were provided by the Melbourne Urology Research Alliance (MURAL) (Lawrence et al., 2018). Tissues were homogenized in Qiazol (QIAGEN) with a Precellys24 Tissue Homogenizer (Bertin Technologies) and total RNA was extracted using a miRNeasy Mini Kit (QIAGEN), according to the manufacturer's instructions.

Quantitative RT-PCR (qRT-PCR) analysis of mRNA

Total RNA was treated with Turbo DNA-free kit (Invitrogen), and reverse transcribed using iScript Reverse Transcriptase Supermix kit (Bio-Rad). qRT-PCR was performed using iQ SYBR Green Supermix (Bio-Rad) in triplicate as described previously (Moore et al., 2012). GAPDH levels were used for normalization of qRT-PCR data. Primer sequences are provided in Table S6.

qRT-PCR analysis of miR-194

Total RNA (100 ng) was reverse transcribed using the TaqMan MicroRNA Reverse Transcription Kit (Applied Biosystems) and Taqman Microarray Assays (Thermo Fisher Scientific). Quantitation of miR-194, U6 and RNU44 was done by qRT-PCR using Taqman Microarray Assays (Thermo Fisher Scientific) and TaqMan Universal Master Mix II, no UNG (Applied Biosystems) on a CFX384 real-time PCR detection system (Bio-Rad). MiR-194 expression was normalized to expression of U6 (cell lines) or the geometric mean of U6 and RNU44 (PDX tissues).

Proliferation and cell viability assays

Proliferation curves for cell lines treated with LNA miRNA inhibitors were performed using the Trypan blue exclusion assay. Cells were seeded at 1×10^4 (PC3) or 4.5×10^4 (LNCaP-MR42D, LNCaP-MR49F, LNCaP) in 12-well plates and transfected in suspension with 12.5 or 6.25 nM miR LNA inhibitor using RNAiMAX (Invitrogen). Live and dead cells were quantified at indicated time points using Trypan blue.

For cell viability assays, LNCaP-MR42D or LNCaP cells were seeded at 4×10^3 cells/well in 96-well plates and transfected in suspension with 12.5 or 6.25nM miR LNA inhibitor using RNAiMAX (Invitrogen). Cell viability was assesses using the Cell Titer-Glo Luminescent Cell Viability Assay (Promega) according to manufacturer's recommendations.

Neurite length measurement

Length of neurite extensions were measured using the Simple Neurite Tracer plugin (Longair et al., 2011) for Fiji/ImageJ (Schindelin et al., 2012). Neurite lengths were measured from $\geq$ 3 images per replicate. Representative images with overlaid traces were generated using the NeuronJ plugin (Meijering et al., 2004) for Fiji/ImageJ.

Western blots

Protein extraction from cells using RIPA buffer and western blotting was done as described previously (Moore et al., 2012). Primary antibodies used in western blotting were FOXA1 (Abcam, Ab23738), ERK (Cell Signaling Technology, 9102), phospho-ERK (Cell Signaling Technology, 9101) and GAPDH (Millipore, MAB374). Secondary antibodies used were HRP conjugated anti-rabbit and anti-mouse IgG (Dako). Immunoreactive bands were visualized using Clarity Western ECL Substrate (Bio-Rad).

Chromatin immunoprecipitation (ChIP)-sequencing

LNCaP cells were seeded in 15cm plates and transfected in solution with 50 nM miRNA mimic (miR-194 or negative control; Shanghai GenePharma) using RNAiMAX (Invitrogen). After 72 hours, cells were fixed with formaldehyde and chromatin immunoprecipitation (ChIP) was performed essentially as described previously (Paltoglou et al., 2017). Anti-FOXA1 (ab23738, Abcam) was used for ChIP. ChIP-sequencing was performed on 3 biological replicates each of LNCaP cells transfected with miR-194 or negative control. ChIP-sequencing libraries were constructed from 5 ng of DNA (ChIP-enriched or input) using an Illumina TruSeq ChIP Library Prep kit (Illumina) and sequenced on the Illumina Nextseq 500 platform using the single end protocol with a read length of 75 at the South Australian Health and Medical Research Institute Genomics Facility. Mapping and processing of fastq files were performed as described previously (Chan et al., 2015). Differential binding analysis was performed using the DiffBind package (Ross-Innes et al., 2012).

Organoid transfections

Organoids were transfected with miR LNA inhibitors essentially as described previously (Broutier et al., 2016). Briefly, organoid were collected and 50,000 cells were resuspended in 450µl of organoid culture media and 50 µL of transfection mix containing RNAiMAX with 25, 100, and 250 nM miR-194 or NC LNA inhibitor. Cells were centrifuged in a pre-warmed centrifuge at 32°C, 600 g for 1h. After centrifuging, cells were incubated in a tissue culture incubator at 37°C for 2-4h and then collected in 1.5ml centrifuge tubes by centrifugation at 300 g for 5 min at room temperature. Cell pellets were resuspended in 50 ul Matrigel and seeded out in 10 µL matrigel discs in 96-well plates. Plates were inverted and incubated at 37°C for 15 minutes to allow Matrigel to solidify, then overlaid with 100mL of organoid culture medium. Organoid forming efficiency was determined at 7 days post-transfection as described previously (Lawrence et al., 2018). Organoid viability was assessed at 7 days post-transfection using the CellTiter-Glo® Luminescent Cell Viability Assay kit (Promega), as per the manufacturer's instructions.

Phase contrast images of organoids were obtained with a Leica DM IL LED microscope with Leica DFC425 C digital camera. For immunohistochemistry, organoids were pelleted in agar, then formalin-fixed and paraffin embedded. Sections were stained using a Leica BOND-MAX-TM autostainer with BondTM epitope retrieval 1 or 2 and the Bond Refine Detection Kit (Leica). Primary antibodies are listed in Table S5.

QUANTIFICATION AND STATISTICAL ANALYSIS

Statistical analyses for grouped quantitative data were carried out using two-tailed unpaired t test or ANOVA (GraphPad Prism 8). The relationships between activity scores were determined using Pearson's correlation coefficient (Graphpad Prism 8). Further details of statistical tests are provided in the figure legends. Statistical significance was defined as $p < 0.05$.